Master's Thesis

A gas sensor based on the suspended carbon nanomesh functionalized with metal oxide nanowires and their junctions

Seungwook Lee

Department of Mechanical Engineering

Graduate School of UNIST

2019

A gas sensor based on the suspended carbon nanomesh functionalized with metal oxide nanowires and their junctions

Seungwook Lee

Department of Mechanical Engineering

Graduate School of UNIST

A gas sensor based on the suspended carbon nanomesh functionalized with metal oxide nanowires and their junctions

A thesis/dissertation
submitted to the Graduate School of UNIST
in partial fulfillment of the
requirements for the degree of
Master of Science

Seungwook Lee

06/14/2019
Approved by

Advisor
Heungjoo Shin

A gas sensor based on the suspended carbon nanomesh functionalized with metal oxide nanowires and their junctions

Seungwook Lee

This certifies that the thesis of Seungwook Lee is approved.

06/14/2019

signature

Advisor: Heungjoo Shin

signature

Jaesung Jang

signature

Hooneui Jeong

signature

Abstract

This study reports the development of a high-performance gas sensor platform based on the suspended carbon nanomesh (line width ~300nm, thickness ~ 400nm) functionalized with 1-D metal oxide nanowires (NWs). Thanks to the unique nanomesh structure, 1-D metal oxide NWs grown from each line of the mesh cross each other making junctions. These junctions provide an additional gas sensing mechanism to the sensor result in higher gas response and a wider sensing range. In this research, the sensor was constructed by integrating ZnO nanowires (diameter ~ 30 - 70nm, length ~3 μm), and high sensitivity (200.59ppb^{-1}) and wide detection range (50ppb – 5ppm) were confirmed to NO_2 gas. Furthermore, the suspended carbon nanomesh, which is backbone of the sensor platform, provides enhanced mass transfer, high surface to volume ratio and elimination of noise from the bottom substrate. Thanks to these properties, fast response and recovery and reliability of the sensor were also confirmed. The fabrication of this sensor platform is a wafer-level fabrication process including carbon-microelectromechanical systems(C-MEMS) and hydrothermal method making the proposed sensor platform cost-effective. Most of all, this study is about the gas sensor platform, so that it can be a cornerstone of further studies simply by employing other sensing materials. Thus, the proposed gas sensor that based on the suspended carbon nanomesh functionalized with metal oxide nanowires and their junctions suggests a novel, high-performance, reliable and cost-effective sensor platform.

Contents

1 Introduction

1.1 The necessity of gas sensor

Over the past several decades, the development of gas sensors has attracted much attention as an application of intelligent systems for the development of industry and technology. So far, the development of gas sensors has been applied as an important factor in technological development in various fields such as 'factory production', 'automobile industry', 'medical technology', 'environmental protection' and 'industrial safety management' [1-8]. Furthermore, research is still being actively pursued to develop higher performance gas sensors to meet the needs of the future industry. These recent research trends focus on factors that are important indicators of gas sensor performance such as high sensitivity, reliable sensitivity, fast response and recovery times, wide sensing range and low power consumption [9,10].

The development of nanotechnology opened many possibilities for the development of sensor technology [11-13]. Especially, in the gas sensor market, the sensor has been miniaturized up to the micro-nano level, enabling the sensor to be portable and low-power consuming [14,15]. Besides, as many fabrication methods synthesizing nanostructures of gas sensing materials have been revealed [13,16-18], the performance of sensors is greatly improved by employing various nanostructures. Nanostructures like nanowires(1-D) [19-21], nanoflakes(2-D) [22-24] or nanospheres [25,26] have an extremely high aspect ratio, making it advantageous that more gas molecules are effectively adsorbed and desorbed.

Although various technologies are developed and gas sensors continue to evolve, most of the gas sensor technologies suffer from a trade-off between sensor performance and fabrication cost,

resulting in a gap between actual industrial applications and research development [10,27]. In particular, nano-level fabrication processes usually involve expensive types of equipment and high process costs. In this situation, it is important to develop a gas sensor that is reasonable in terms of performance as well as manufacturing cost.

1.2 Types of gas sensors

Over the past several decades, gas sensors have evolved based on a variety of methodologies and sensing materials. Gas sensors that have been studied to date can be categorized into some representative types which include catalytic combustion[28,29], thermal conductivity[30], electrochemical[31-33], optical[34,35] and semiconductor[36-39] depending on the operating principle and sensing material. Each type of gas sensor has its unique advantages and disadvantages. Further researches are underway to overcome these shortcomings and to maximize the benefits. In table 1, various types of gas sensors are compared concerning sensitivity, selectivity, response time, stability, and cost, which are typical parameters for evaluating the performance of gas sensors [40].

Parameters	**Types of gas sensors**				
	Catalytic combustion	**Thermal conductivity**	**Electrochemical**	**Optical**	**Semiconductor**
Sensitivity	Good	Poor	Good	Good	Excellent
Selectivity	Poor	Poor	Good	Poor	Fair
Response time	Good	Good	Fair	Good	Excellent
Stability	Good	Good	Poor	Good	Good
Cost	Excellent	Good	Good	Poor	Excellent

Table 1 Comparison of conventional types of gas sensor. Table is reproduced from – A. Dey [40].

Recently, researches on gas sensors are relatively more active for semiconductor metal oxide-based gas sensors. Thanks to its high sensitivity, fast response time and good stability, the gas sensing ability are promising. Although the selectivity is somewhat deteriorated for certain gases, recent researches such as doping noble metal on a semiconductor metal oxide [41,42] or synthesizing a specific nanostructure [43] have improved these disadvantages. Therefore, the semiconductor metal oxide-based gas sensor is attracting more attention as a method to overcome the limitation of other conventional types of gas sensors.

1.3 Metal oxide-based gas sensors

1.3.1 Semiconductor metal oxide

The development of gas sensors has been greatly influenced by the development trends of industry and technology. In the meantime, gas sensors were used to detect flammable and explosive industrial gases that were needed for safety purposes at industrial sites. However, over the last few decades, as the applications of gas sensors have expanded to include biomedical, environmental and chemical applications, gas sensors which can be applied to diverse environments and gases are needed. In particular, there is a growing demand for detect and control systems for gases such as NO_2, SO_2, CO, CH_4, and H_2S and various VOCs gases such as benzene, acetone, and ethanol which are highly related to our environments and human health. These toxic gases require careful precautions since it can cause not only environmental problems but also problems in the human heart, respiratory system and nerve system even at relatively low concentrations [44]. In this situation, metal oxide-based gas sensors arise as one of the ideal gas sensors [45]. As described in Table 1, the metal oxide gas sensor is an excellent

gas sensor in terms of sensing performance and manufacturing cost. Besides, metal oxide gas sensors can detect various gases including these toxic and hazardous gases. For this reason, researches on metal oxide gas sensors are being actively conducted currently to further improve their sensing performances.

1.3.2 Gas sensing mechanism

Semiconductor metal oxide is divided into two types according to the gas detection principle. Metal oxides such as SnO_2 and ZnO, which have been studied extensively as gas sensors so far, are n-type metal oxide and materials such as TiO_2 In_2O_3 are p-type metal oxide [46-50]. In the case of n-type metal oxide, the electrons generated by oxygen vacancy are considered as carriers, while for p-type metal oxide, holes are considered as carriers [51,52]. Due to differences in these models, they are divided into n-type and p-type, respectively. Figure 1 shows the basic structure of n-type and p-type metal oxides.

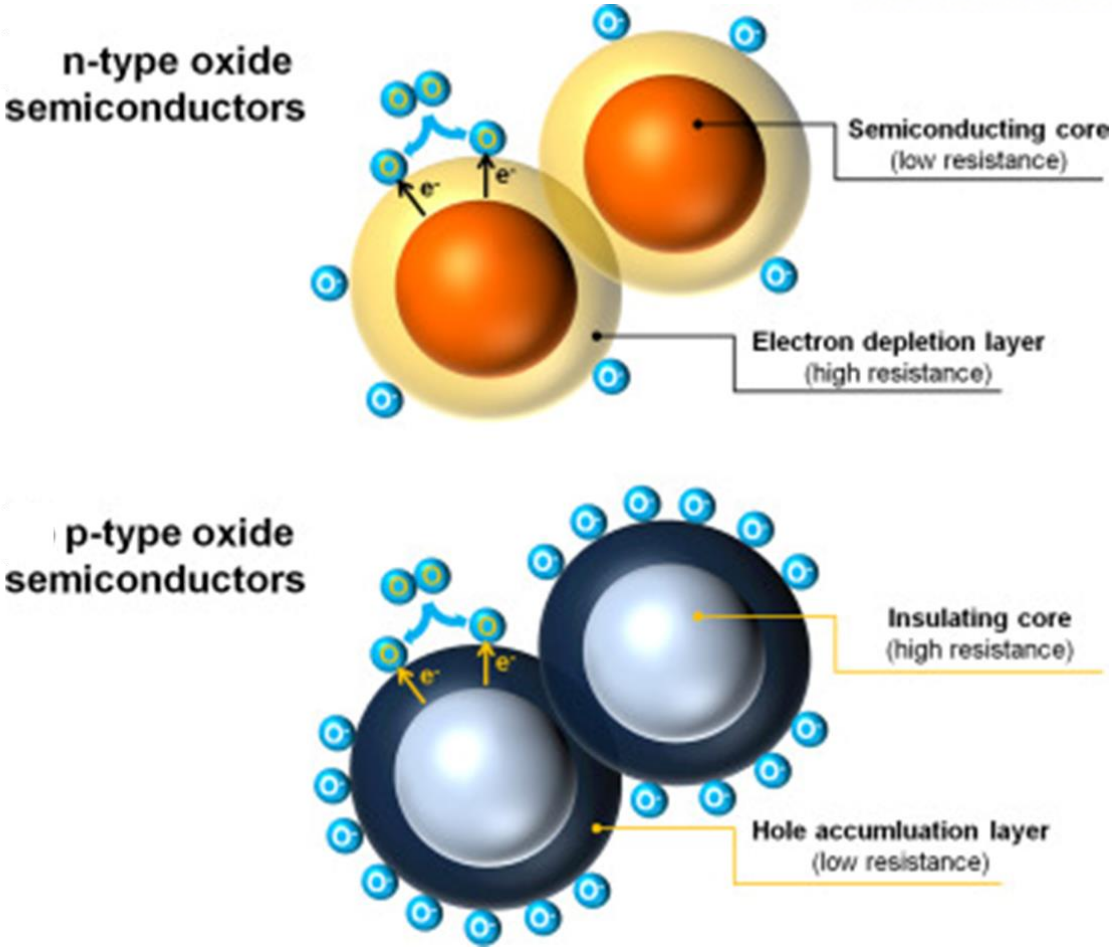

Figure 1. Schematic images of core-shell configurations of n-type and p-type metal oxides [52].

The operation of a gas sensor through a metal oxide is achieved by the action of adsorbed oxygen molecules on the metal oxide surface and the target gas that affects these adsorbed oxygens. Based on N-type metal oxide, a metal oxide crystalline surface can adsorb the oxygen molecules. First, oxygen molecules are physically adsorbed on the n-type metal oxide surface and pull electrons from the semiconducting core which is relatively conductive and hold it. As a result, oxygen molecules are now chemically adsorbed on the surface as - state. Also, since each oxygen is holding electrons, an electron depletion layer is formed near the metal oxide surface [17,40,52]. Some specific gases act on the oxygen adsorbed on the surfaces or their vacancies. As the target gas reacts with the metal oxide surface and the adsorbed oxygen concentration changes, the thickness of the formed electron depletion

layer also changes. This change in the layer thickness of the metal oxide surface can be interpreted as a change in the conductivity of the metal oxide body. Thus, the reaction of the target gas on the surface oxygens can be sensed simply by recording the electrical resistance change of the sensor.

The target gas is divided into oxidizing gas and reducing gas depending on the reaction method on the surface of the metal oxide. Based on the n-type metal oxide, the oxidizing gas increases the thickness of the electron depletion layer by further increasing the oxygen density adsorbed on the metal oxide surface. Therefore, the resistance of the sensor is increased. The reducing gas works oppositely. In the case of p-type metal oxide, since the surface layer that changes by oxidizing and reducing gas is a hole accumulation layer, the effect of resistance increase and decrease is opposite. Figure 2 shows the reaction principle of the basic n-type semiconductor metal oxide gas.

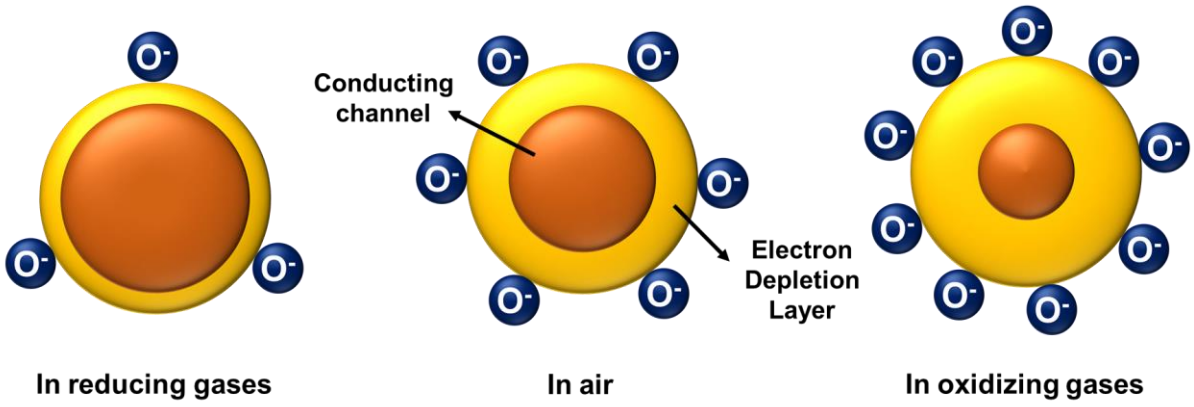

Figure 2. Schematic images of changes in electron depletion layer of n-type metal oxide and its reaction to reducing and oxidizing gases.

Due to the nature of the layer formed near the surface of each type of metal oxide, there happens a difference in the ease of gas sensing reaction between p-type and n-type [52]. On the surface of the n-type metal oxide, a region with high resistance is formed due to the electron depletion layer. On the other hand, for the p-type metal oxide, a hole accumulation layer is formed on the surface. That

is, in the case of p-type, a bulky core has low conductivity and a thin surface layer has high conductivity which is contradictory effects respect to the value of the resistance. As a result, the difference in resistance between the core and the surface layer may not be obvious in the case of the p-type metal oxide. Therefore, if the sensor dimension is not ideal, the sensing performance of the sensor can decay due to this effect. For this reason, n-type metal oxide has been frequently adopted in the metal oxide gas sensor research field until now. Figure 3 illustrates the researches of the n-type and p-type metal oxide gas sensor.

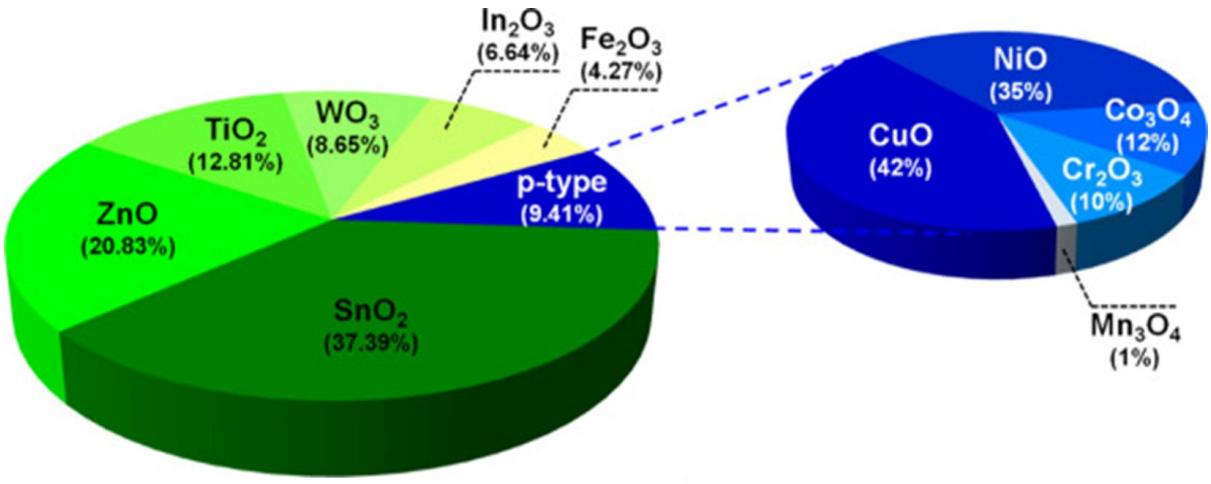

Figure 3. Studies on various metal oxides in the gas sensor field [52].

1.3.3 Various metal oxide nanostructures

Another advantage of metal oxide gas sensor applications lies in the various nanostructures of metal oxides. When the size level of the sensing material is reduced into the nanoscale, it has an extremely high surface-to-volume ratio, which is more advantageous for gas sensing [53,54]. In the nanoscale level, some unique characteristics that cannot be expected from a macroscale appear.

Especially, metal oxide-based nanostructures can be synthesized relatively easily compared to other materials, and the shape and parameters of the nanostructure can be tuned through various controls [55-57]. As nanoscale process technology has been developed by advances in MEMS (Micro Electro Mechanical System) technology, research on metal oxides which have such nanostructures has been vigorously accelerated. Advances in MEMS technology have opened up more possibilities for studying metal oxide-based gas sensors, synergizing with each other and evolving further [58,59].

2-D thin film metal oxide

A 2-D thin film metal oxide is one of the most basic metal oxide nanostructures [60,61]. It has a high surface-to-volume ratio and a large surface area. A 2-D metal oxide is usually tuned to a few tens of nanometers thick or less to achieve reasonable sensor performance, while the width can be varied from several tens to several millimeters. Although 2-D thin film metal oxide has a relatively low surface-to-volume ratio compared to nanoparticles or 1-D nanowires-based metal oxide, it is simple to synthesize, easy to adjust parameters, and easily scalable. Thanks to these eases of fabrication and control, the cost of manufacturing the sensor can be remarkably reduced. Besides, it is the structure that can easily try the junction structure with other metal oxides or doping of noble metal [62,63]. Therefore, in a future study of a metal oxide-based gas sensor, a 2-D thin film structure is the most basic form and has been studied steadily as a cornerstone for various application studies.

Figure 4 describes a gas sensor based on Ultrathin SnO_2 nanosheets [64]. In this study, Ultrathin SnO_2 nanosheets were fabricated using the hydrothermal method and reactivity to formaldehyde gas was confirmed. SnO_2 is an n-type metal oxide semiconducting material that has a wide bandgap (~3.6 eV). In this research, the SnO_2 nanosheet with a uniform thickness in the range of

10-30 nm is synthesized. These nanosheets are synthesized by the hydrothermal method with reagents including $SnCl_2 \cdot 2H_2O$, NaOH, and CTAB. The synthesized SnO_2 nanosheets were dried, dispersed in DI water, and dip-coated onto a gas sensor platform. Employed sensor platform was a ceramic tube with integrated Ni-Cr heater (diameter = 1.35mm, length = 4mm).

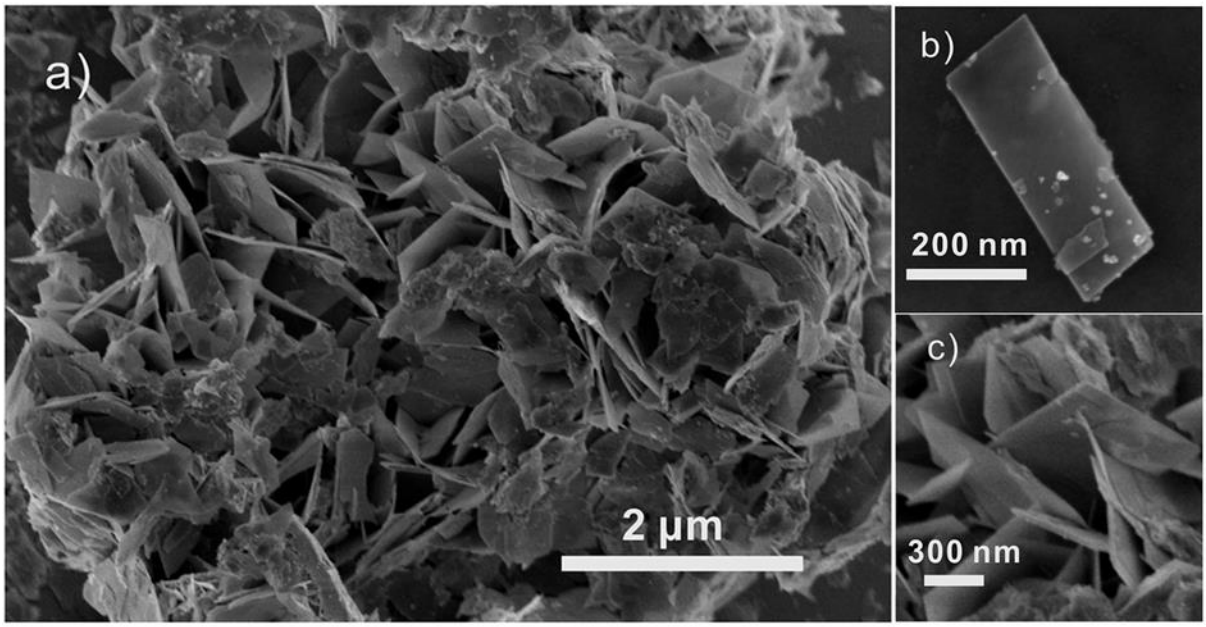

Figure 4. SEM images of the ultrathin SnO_2 nanosheets (a) low-magnification (b,c) an enlarged SEM image [64].

Figure 5 depicts sensor performance and sensor response and recovery time for 5-1000 ppm formaldehyde in SnO_2 nanosheets. Very rapid response and recovery times due to the nature of the SnO_2 nanosheet, which is very thin and has a very high surface area.

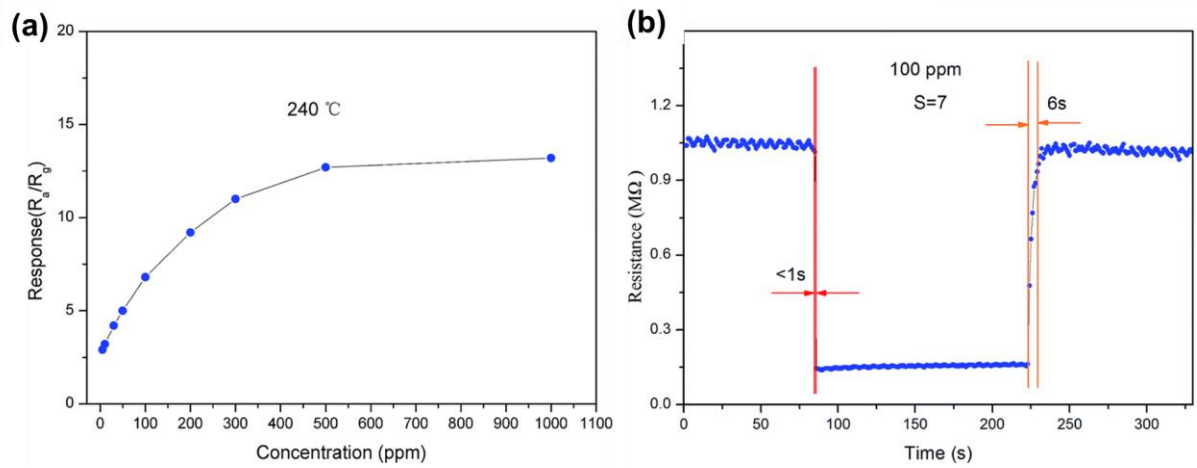

Figure 5. Gas sensing performance of the ultrathin SnO_2 nanosheets sensor (a) Gas response versus gas concentration graph (b) The resistance changes of the ultrathin SnO_2 nanosheets sensors to 100 ppm CH_2O at 240 °C [64].

1-D Nanowire

Despite the many advantages of 2-D nanostructures, 1-D nanowires have a structure that further maximizes these advantages. It has a more maximized surface-to-volume ratio, and the volume itself is a smaller nanostructure, resulting in a more sensitive response. A number of methodologies have been discovered for the easy fabrication of metal oxide nanowires through various studies [65-67]. Among them, the most representative methods are the hydrothermal method [68]. With this methodology, the metal oxide nanowire can be directly integrated into any shape, away from the structural constraints of the sensor. In addition, the hydrothermal method is easy and simple to process and low cost. Thanks to these characteristics, 1-D nanowire structures has been studied as a steady structure of the most frequently employed in the metal oxide gas sensor research.

Figure 6 shows a ZnO nanowire-based gas sensor [69]. ZnO is an n-type metal oxide semiconducting material which has a wide bandgap (~3.37 eV). ZnO NWs were synthesized by the

hydrothermal method on 5 nm thick sputter-deposited ZnO seed. The ZnO NWs were about 400 nm in length and 70 nm in diameter. The hydrothermal process was conducted using $Zn(NO_3)_2 \cdot 6H_2O$ and HMTA 25 mM solution at 90°C for 2 hours.

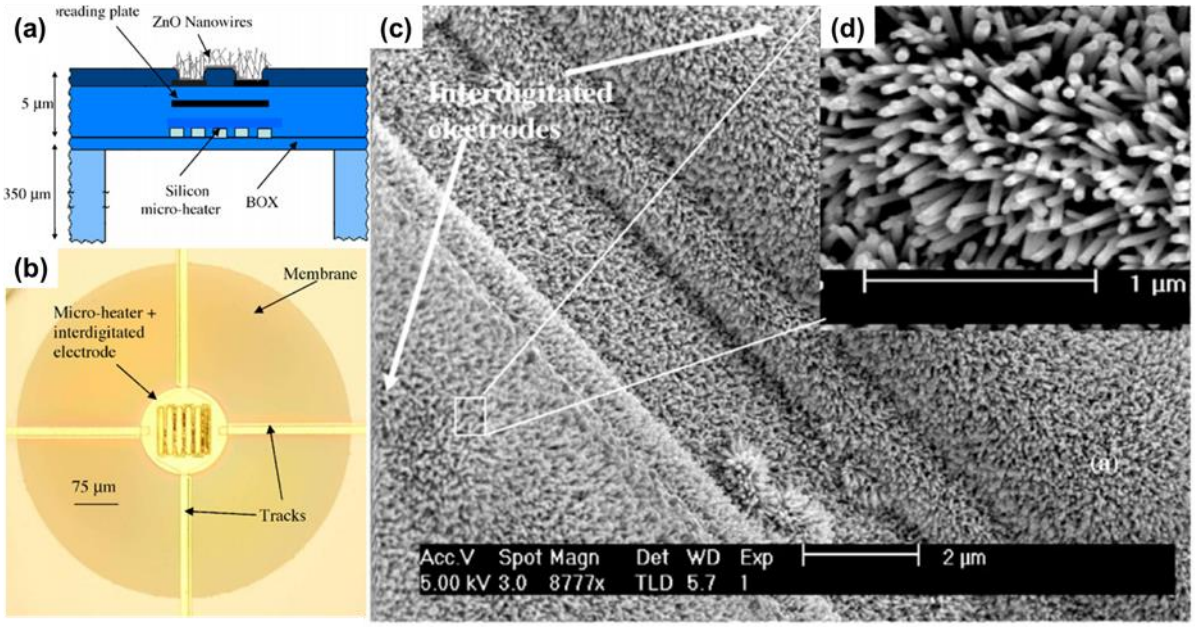

Figure 6 (a) Schematic image of the ultrathin SOI micro-hotplate. (b) An optical microscope image of the micro-hotplate. (c) SEM images of the ZnO NWs on the surface of interdigitated electrode. (d) magnified SEM image of ZnO NWs [69].

The performance of the sensor was measured by sensing the ethanol at 800 ~ 4500 ppm as shown in Figure 7. It has demonstrated high reactivity and reproducible gas sensing performance at operating temperatures of 400°C. Thanks to the NW's structural properties, fast response and recovery times were achieved.

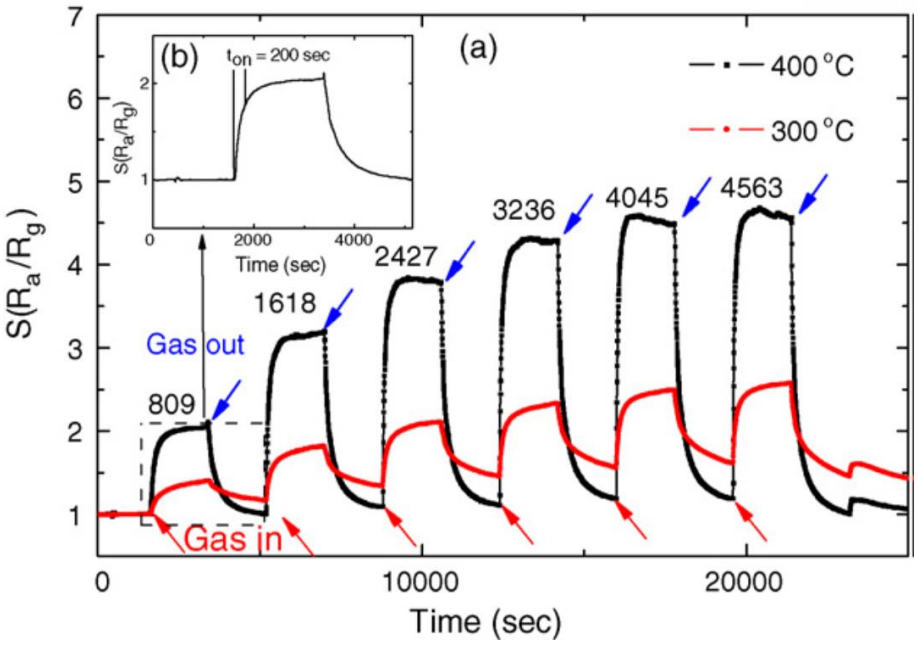

Figure 7 (a) Gas response of the fabricated ZnO NWs ethanol gas sensor at different concentrations at 300°C and 400°c. (b) magnified image of the gas response exposure to 809 ppm ethanol at 400°C [69].

Nanosphere

The nanosphere structure began to attract attention as a way to make a core-shell structure, a hollow nanosphere, as a somewhat special structure. Because very small nanoparticles are agglomerated, they have very high surface-to-volume ratios and extremely high surface active sites. In particular, in the case of a hollow structure with an inner volume empty, very sensitive and fast gas sensing performance can be expected [70,71]. However, the nanosphere is difficult to integrate directly into the sensor platform and is subjected to a transfer process, which makes it difficult to uniformly disperse nanospheres during this process. Also, reproducibility may be low due to such a process. Nevertheless, nanospheres with very small nanometer sizes show very high gas detection performance, so research on this structure is steadily increasing.

Figure 8 summarizes the gas sensor studies with an integrated CuO nanosphere [72]. Copper

oxide (CuO) is a p-type metal oxide semiconductor material with a relatively narrow bandgap of 1.2 eV. The CuO nanosphere synthesis process consists of dissolving 2mmol of $Cu(CH_3COO)_2 \cdot H_2O$ in 25 mL of DMF, adding polyvinyl pyrrolidone (PVP; mw = 30,000) and $NaBH_4$. Thereafter, the Cu_2O nanosphere is synthesized by continuous stirring at a temperature of 90°C. These Cu_2O nanospheres are integrated on a gas sensor platform with a heater-embedded ceramic tube by a dip-coating method to complete the gas sensor. In the case of CuO nanosphere, Cu_2O is converted to CuO through a heat treatment at 500°C to fabricate a gas sensor integrated with CuO nanosphere.

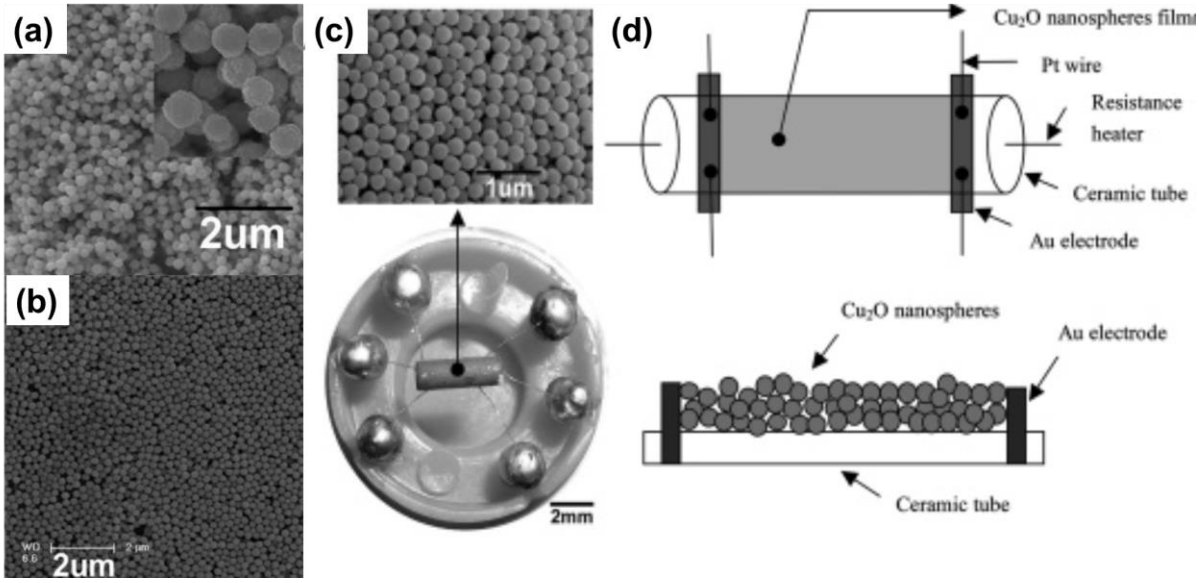

Figure 8. (a) SEM image of as-synthesized CuO nanospheres. (an inset image is magnified CuO nanospheres) (b) SEM image of self-assembled CuO nanospheres (c) Real image of the actual gas sensor and the SEM image of the sensor surface. (d) Schematic image of the structure of a typical Cu_2O nanosphere gas sensor [72].

As shown in Figure 9, the performance of CuO and Cu2O nanosphere gas sensors was measured for alcohol vapor and gasoline. Due to their hollow structure and the characteristics of the nanosphere, the response time of the sensor was very fast, ranging from 15 to 25 s.

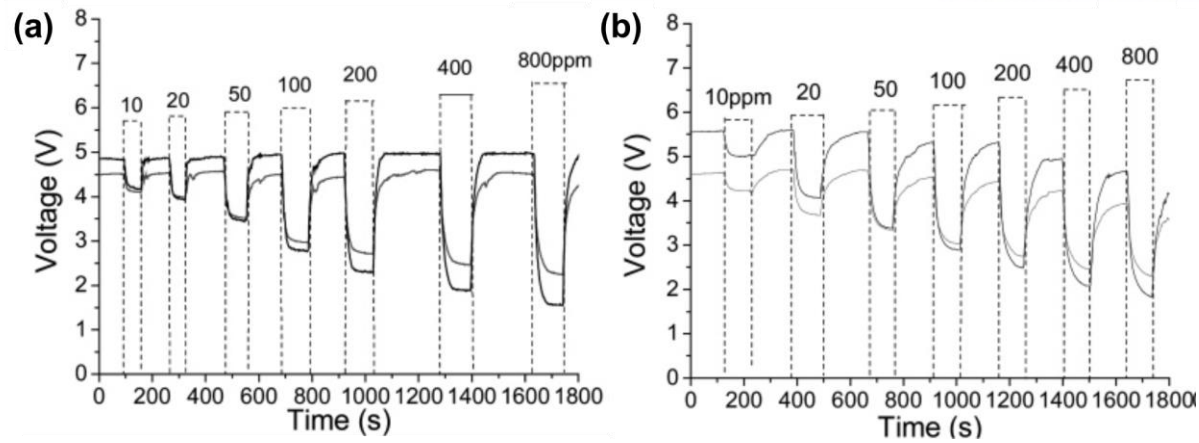

Figure 9. (a) The gas response graph under various concentrations of alcohol at 210°C (b) The gas response graph under various concentrations of oil at 210°C (Black line : Cu_2O / Gray line : CuO) [72].

1.4 Gas sensor structural platforms

A study on the structure of the gas sensor platform as well as the study of the material of the gas sensor. The basic structure of the gas sensor platform as much as the material of the gas sensor has a great influence on the performance of the sensor. In addition, the structure that facilitates easy mass transfer and effective gas access is desirable. In addition, studies have been made on a structure that reduces the power consumption and enhances the sensing performance by miniaturizing the sensor platform size itself. In recent years, a sensor platform in the form of a ceramic tube with an embedded heater coil or a sensor heater stage in the form of a microheater made of a thin metal electrode is widely used [73,74].

1.4.1 Suspended structure

Make a gas sensor suspended is a very good strategy to enhance the performance and properties of a gas sensor [75]. As the sensor material is suspended, the mass transfer is improved, and

good performance including fast sensor response and recovery can be expected. In addition, the effect of a stagnant layer formed by gas molecules can be minimized and free from the noise coming from the substrate, so that a stable signal can be obtained.

Figure 10 describes a study on the fabrication of a gas sensing material in suspended form using a MEMS process [76]. An electrode of the IDA structure is formed by the MEMS process on the SOI wafer. Then, the Fe catalyst is deposited using evaporation and patterned using RIE. On top of this, CNTs are deposited by chemical vapor deposition (CVD) to form a suspended geometry frame. The gas sensing material is evaporated on it to oxidize and remove the CNT. SnO_2, WO_3 NiO and PdO were used as the sensor material, and the performance of the hydrogen reaction of Pd was evaluated.

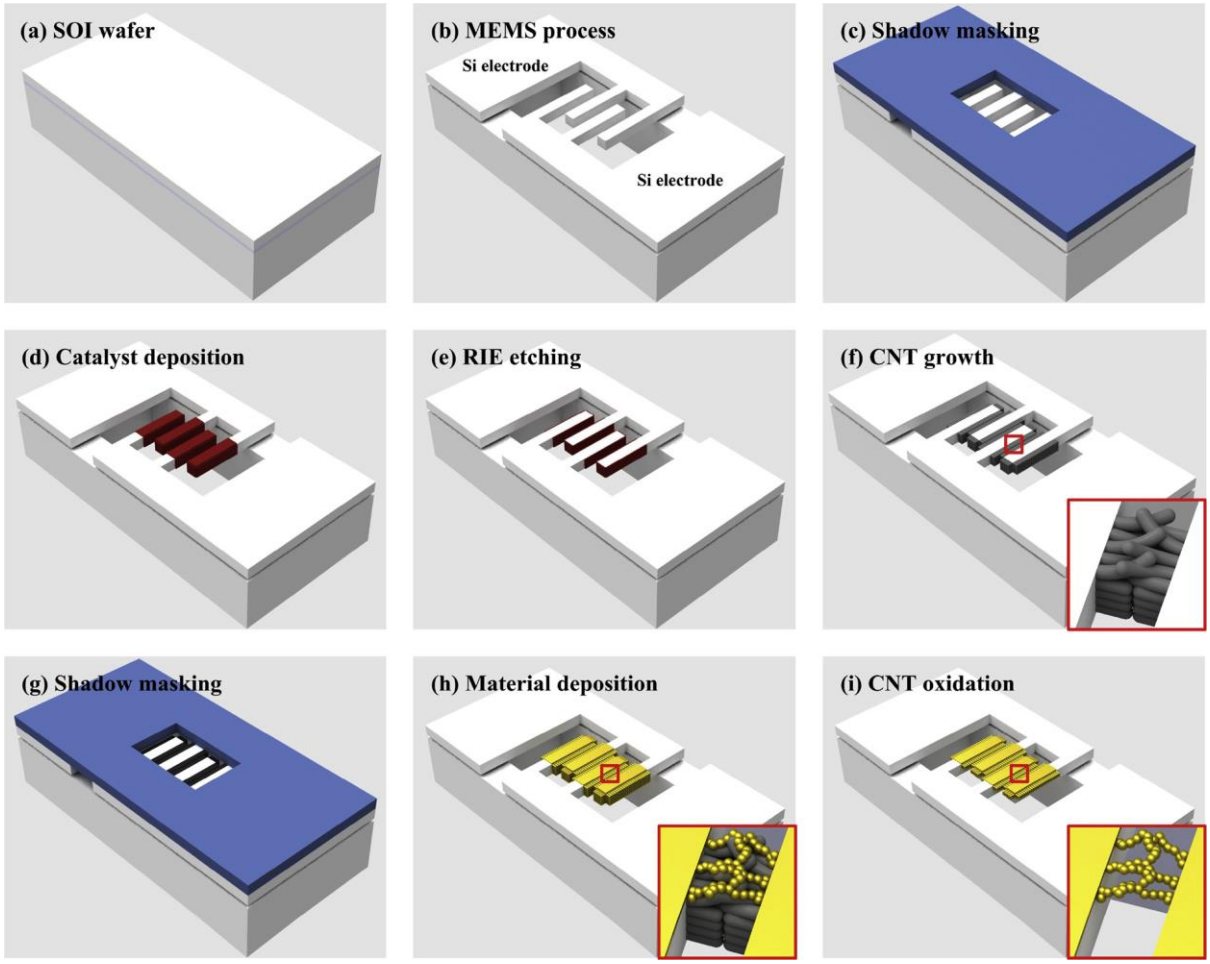

Figure 10. Schematic images of fabrication steps of of suspended nanowires by the CNT sacrificial

template. (a–b) Patterning of the Si electrodes on a SOI wafer via MEMS technology. (c–d) Deposition of the Fe catalyst on the interdigitated Si electrodes (e) The catalyst on the top surface is etched using RIE. (f) Synthesis of CNTs using CVD. (g–h) Deposition of the material of nanowires on the top surface of CNT structure by evaporation. (i) Removal of the CNT template [76].

Figure 11 shows the shape of the processed suspended SnO_2 wire and the hydrogen response graph of PdO. It can be seen that the suspended structure remains well after CNT removal. The performance of the gas sensor shows fast recovery and response due to the nature of the suspended structure.

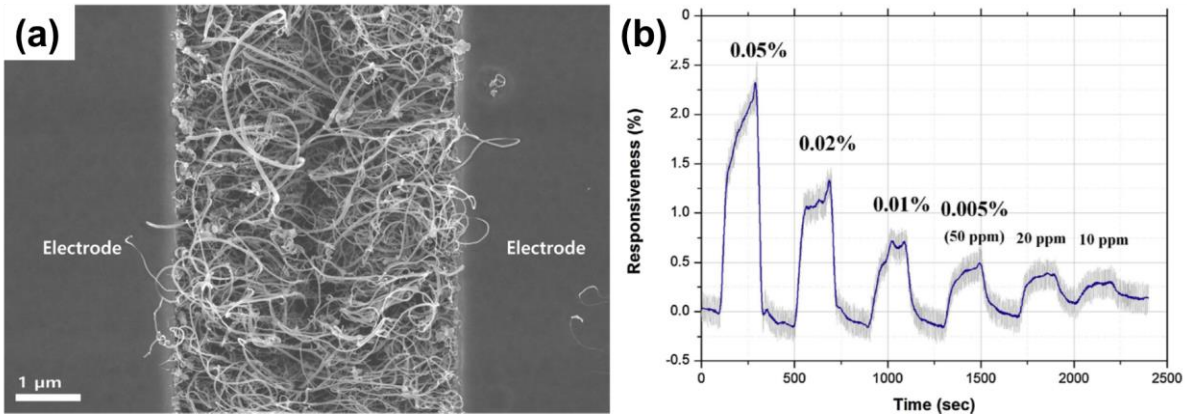

Figure 11. (a)The fabricated suspended nanowire structure is same with that of original CNTs. (b) The responsiveness vs time graph for Pd nanowires under different concentrations of H_2 [76].

1.4.2 Metal oxide junction structure

Studies on the 1-D metal oxide have been studied extensively, and studies on junctions between metal oxide NW structures have been actively conducted [77,78]. Recently, it has been reported that the performance of the NWs network with junction structure is better than that of a single ZnO NW due to the potential barrier modulation effect at the junction of the metal oxide.

Figure 12 shows a comparison of ZnO single wire and ZnO multiple wires with ZnO junctions [78]. They compared the structures of ZnO single NW and multiple ZnO NWs dispersed to have many

junctions.

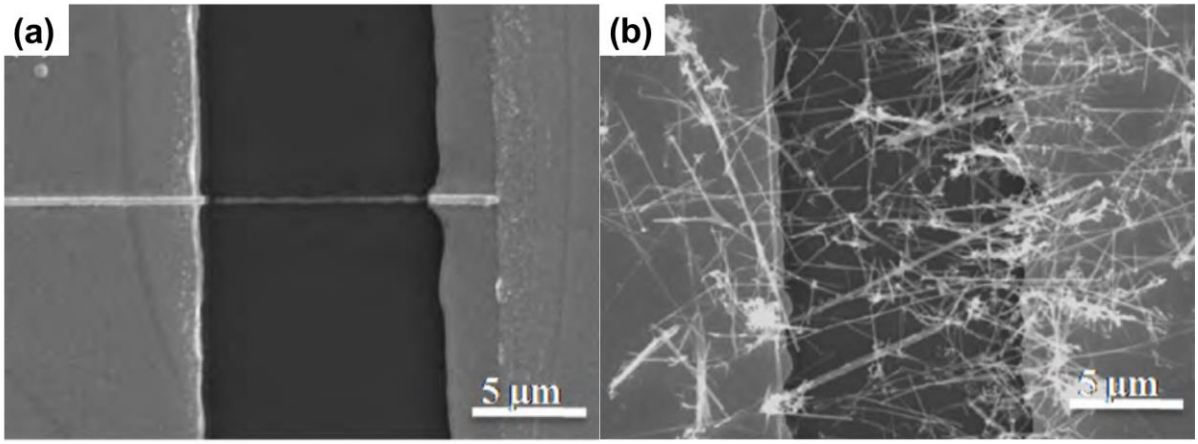

Figure 12 SEM images of (a) the single and (b) multiple ZnO nanowire [78].

As shown in Figure 13, the junction of the metal oxide NW provides an additional current path to the circuit of the gas sensor. In this case, a potential barrier is formed at the ZnO junction, which affects the electron flow through the junction. This results in an additional mechanism to change the overall resistance of the sensor. Therefore, two sensing mechanisms work simultaneously: ‘thickness variation of the conducting channel inside the ZnO NW’ and ‘potential barrier change at the ZnO NWs junction’. This allows for higher gas sensing performance in sensors with junction structures. As shown in the gas sensing results of Figure 13, it can be seen that the ZnO multiwire with junctions shows a higher response to the gas of the same concentration than single ZnO wire.

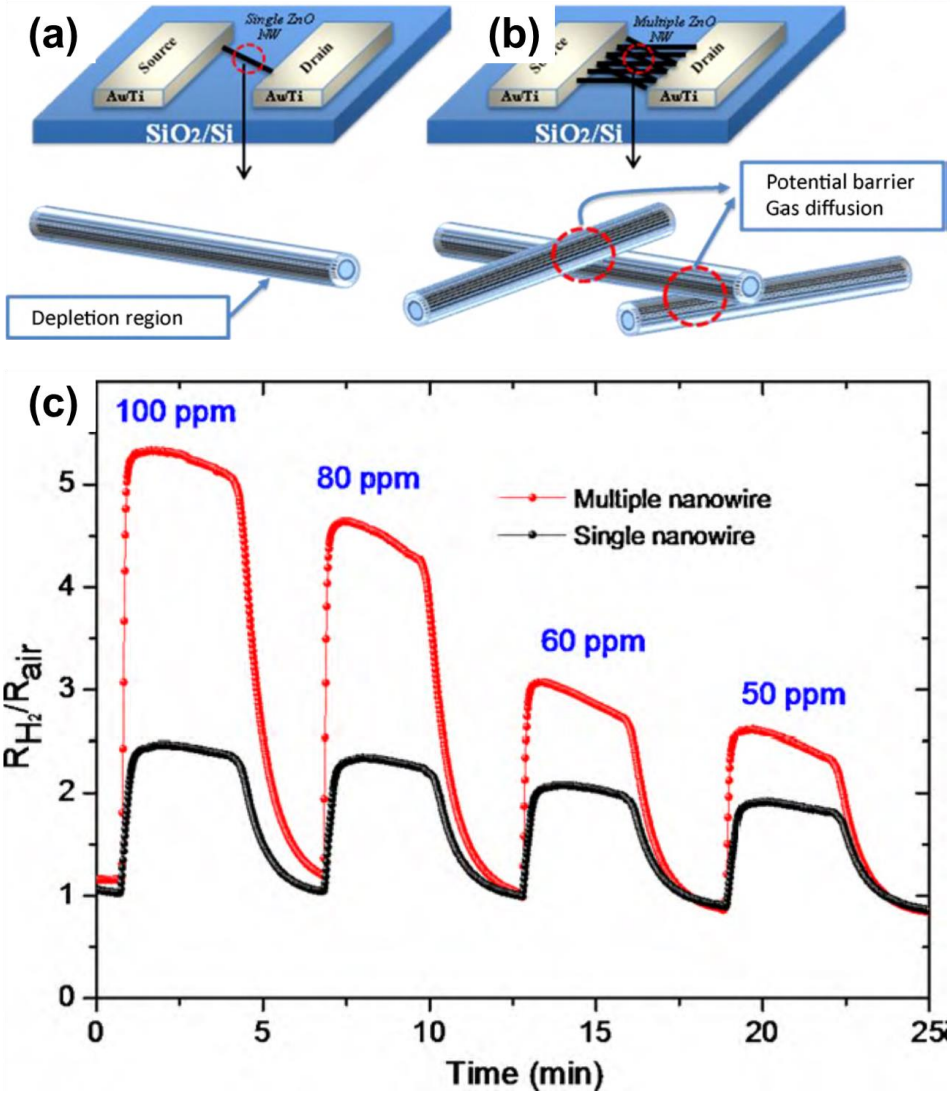

Figure 13. (a,b) Schematic images of the (a) single ZnO nanowire and (b) multiple ZnO nanowires. The red circles indicate ZnO nanowire junctions (c) The gas response graph of the single and multiple nanowire to different H_2 concentration at 200°C [78].

1.4.3 Hierarchical structure

Our research team previously reported on a gas sensor based on a suspended hierarchical nanostructure consists of coexisting two nanoscale structures, that is, a ZnO NWs forest on a carbon nanowire [79]. Conventionally, widely used gas sensor platforms are several mm to several hundreds of μm in size, and the efficiency of nanostructure of sensing material cannot be maximized since the

whole sensor structure is a macro scale. However, by hierarchically integrating the structure of the nanoscale, the sensing performance of the sensor was enhanced by maximizing the advantages of the nanoscale structures. Figure 14 describes our previous work done by our research team that fabricated a gas sensor by integrating a ZnO NW on a suspended carbon nanowire.

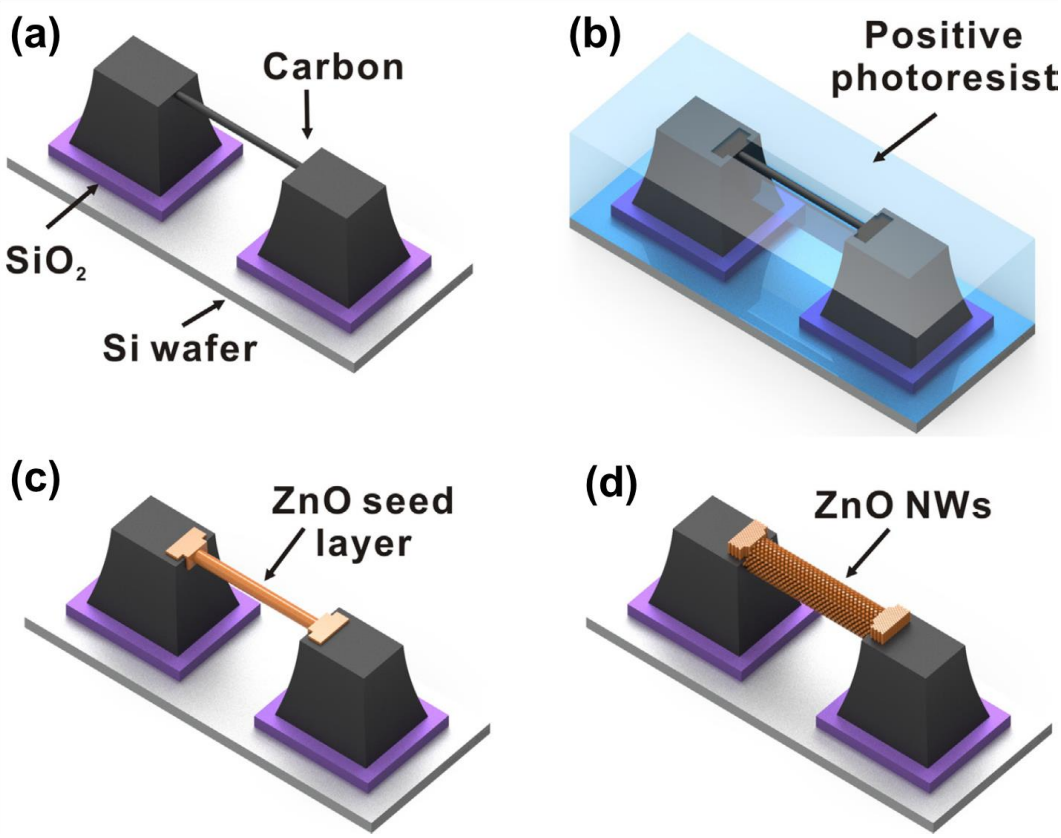

Figure 14 Schematic images of fabrication flow of a gas sensor platform based on a suspended carbon nanowire and selectively grown metal oxide nanowire forest: (a) the suspended carbon nanowire, (b) selectively patterned photoresist. (c) Deposition of ZnO seed layer (d) ZnO hydrothermal [79].

As shown in Figure 15, the sensing material ZnO NWs was successfully grown on the surface of the suspended carbon nanowire. Because the two nanoscale structures form a hierarchical structure, they show a large response and a fast response and recovery time(Figure16). In addition, since the suspended carbon nanowire has a cylindrical structure, ZnO NWs growing on the surface can be radially distributed. This has allowed us to maximize gas accessibility. In addition, all processes can be batch-

fabricated, so the proposed sensor was cost-effective.

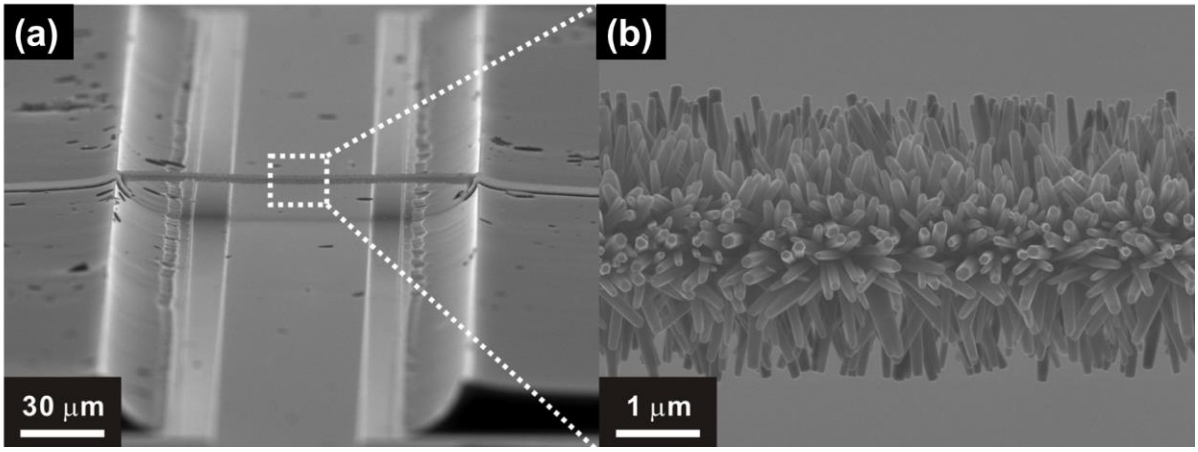

Figure 15. SEM images of a carbon nanowire and selectively grown ZnO nanowire forest [79].

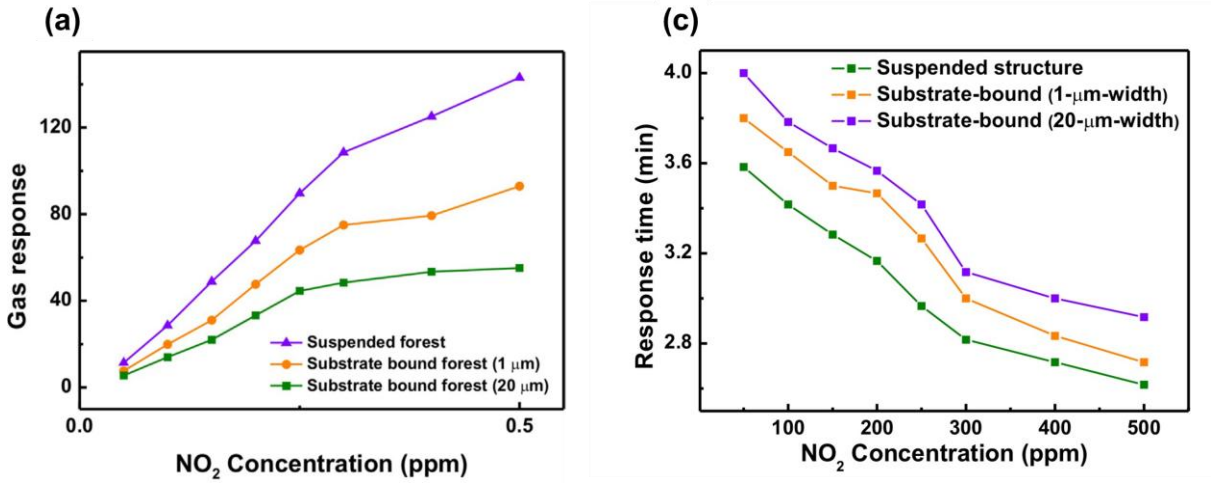

Figure 16. Comparison graph of the (a) gas response versus NO_2 concentration and (b) response time to various NO_2 concentrations at 200°C (Violet line : ZnO nanowire forest on the suspended carbon nanowire / Orange line : ZnO nanowire forest on the 1 μm width of substrate-bound carbon pad / Green line : ZnO nanowire forest on the 20 μm width of substrate-bound carbon pad) [79].

1.5 Thesis outline

In this work, a highly sensitive and reliable gas sensor based on the suspended carbon nanomesh which facilitates metal oxide junction bridge network. Here, ZnO NW is chosen as a sensing

material due to its promising reliability and high sensitivity to various gases and ease of fabrication of high aspect ratio nanowires. Whole fabrication steps are batch fabrication viable so that a cost-effective method. The suspended carbon nanomesh is fabricated via Carbon MEMS(C-MEMS) including successive UV-lithography to pattern the polymer micromesh and pyrolysis to decompose polymer micromesh into the carbon nanomesh [75]. The ZnO NWs are synthesized by the hydrothermal method. By controlling hydrothermal conditions, synthesized nanowires are long enough to make junction bridges as nanowires are grown from each line of the mesh structure. For this gas sensor, gas sensing performances including response, response time, linear sensing range and reproducibility are demonstrated.

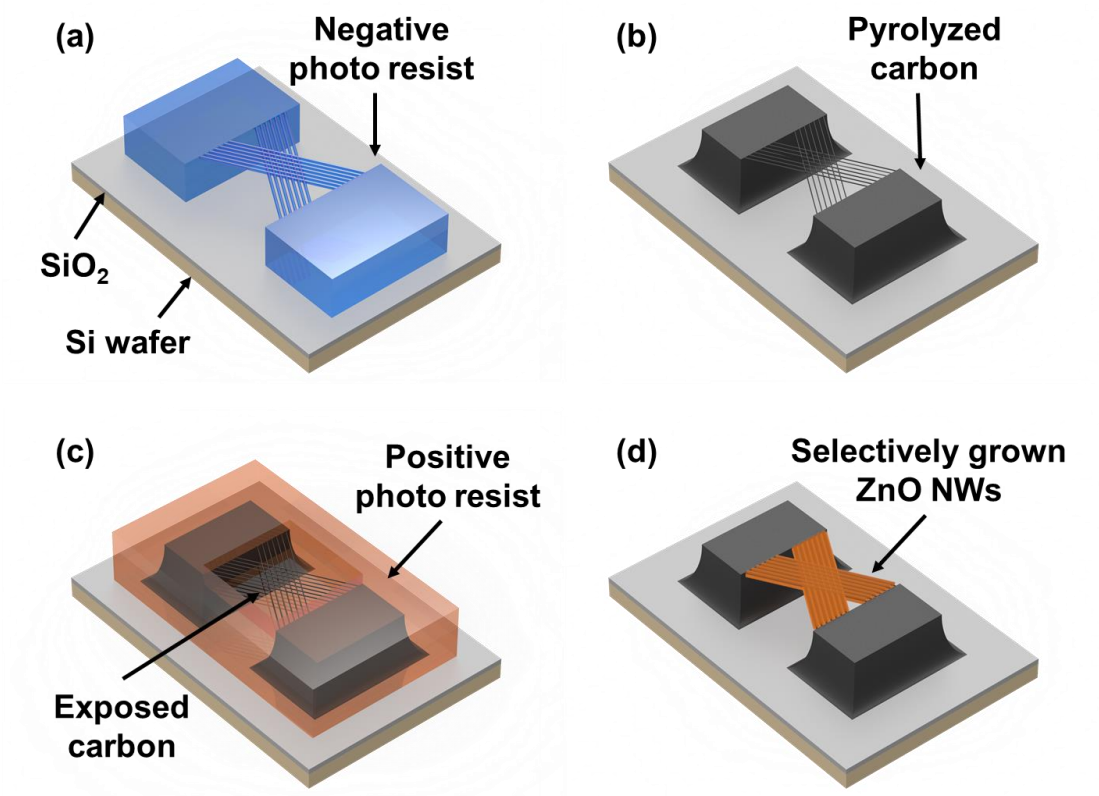

Figure 17. Schematic images of fabrication steps of suspended carbon nanomesh functionalized with ZnO NWs and their junctions. (a) Suspended polymer micromesh (b) Suspended carbon nanomesh (c) Positive photoresist selective opening (d) Selectively integrated ZnO NWs and formation of their junctions

2 Experimental

2.1 An overview of the gas sensor fabrication processes

In this work, a novel gas sensor platform based on suspended carbon nanomesh which facilitates metal oxide NWs junction bridge network is fabricated using C-MEMS and hydrothermal metal oxide growth. A schematic image of the fabrication process is shown in Figure 18. At first, SiO_2 1um / Si wafer is prepared by wet oxidation followed by piranha cleaning. On top of that, the photoresist is spin-coated on the substrate. Then, Polymer micromesh is patterned by two successive UV-lithography processes. After the development process, the suspended micromesh could be defined at once. Then, by the pyrolysis process using the furnace, the suspended polymer micromesh changed into suspended carbon nanomesh. After that, UV-lithography is performed once more to selectively deposit ZnO seed on the mesh portion. ZnO NWs are grown by the hydrothermal method on selectively deposited ZnO seeds. A detailed description of each step is referred to in each section of this thesis.

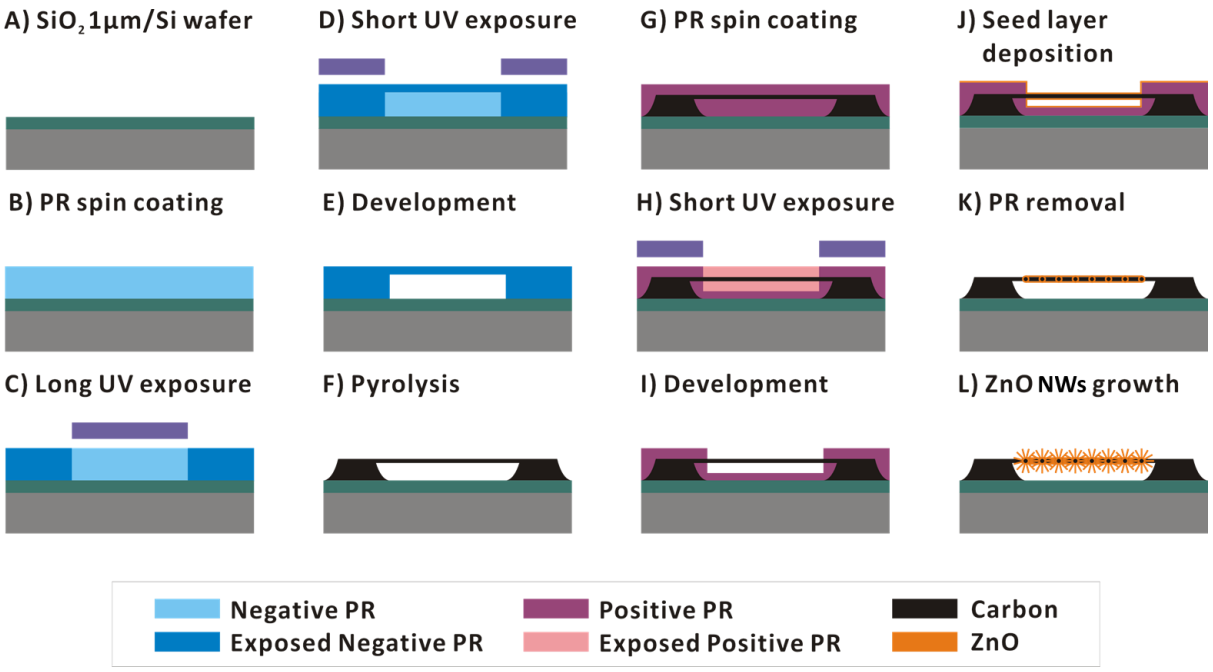

Figure 18. Schematic of the fabrication steps of suspended carbon nanomesh functionalized with ZnO

NW junction bridge network.

2.2 The fabrication of the suspended carbon nanomesh using C-MEMS

The fabrication steps of the suspended carbon nanomesh are illustrated in Figure 18 from A) to F). 1μm-thick SiO_2 layer was thermally grown on bare Si wafer (p-type, boron-doped, 5-20 Ω·cm, 660-700μm thick, LG siltron Co., Ltd., Korea) by wet oxidation. Before coating the photoresist on this wafer, it was cleaned with a hot piranha solution (H_2O_2:H_2SO_4=1:4, 200°C) to remove contaminants on the wafer surface. The suspended polymer micromesh was patterned by two successive UV-lithography. For patterning of the polymer structure, 25μm-thick photoresist (SU-8 2025, Microchem. Corp., USA) film was spin-coated on the wafer and soft-baked at 95°C for 7 minutes. To define the post that supports the suspended mesh parts, post structure was exposed(200mJ/cm^2) enough to polymerize top to bottom. After that, for suspended mesh parts, the photoresist was exposed(10mJ/cm^2) slightly to polymerize only the top shallow region of the photoresist film. After the hard baking process at 95°C for 6 minutes, the suspended polymer micromesh is defined by a single development process. Then, this structure is pyrolyzed in a vacuum furnace (1°C/min ramping rate, hold at 700°C for 1 hour) to convert polymer into carbon. The pyrolysis process accompanies dramatical volume reduction (~97%). So, the microscale structure could be converted into a nanoscale structure. In this research, suspended polymer micromesh was turned into suspended carbon nanomesh.

Figure 19 describes a previous study of our research team about the fabrication of suspended carbon nanowires [75]. Cutting the suspended carbon nanowire through FIB milling shows that the internal stress is hanging upwards. This makes it possible to maintain the suspended structure stably

without bending down the structure during fabrication of the 3-D monolithic suspended carbon nanostructure via pyrolysis.

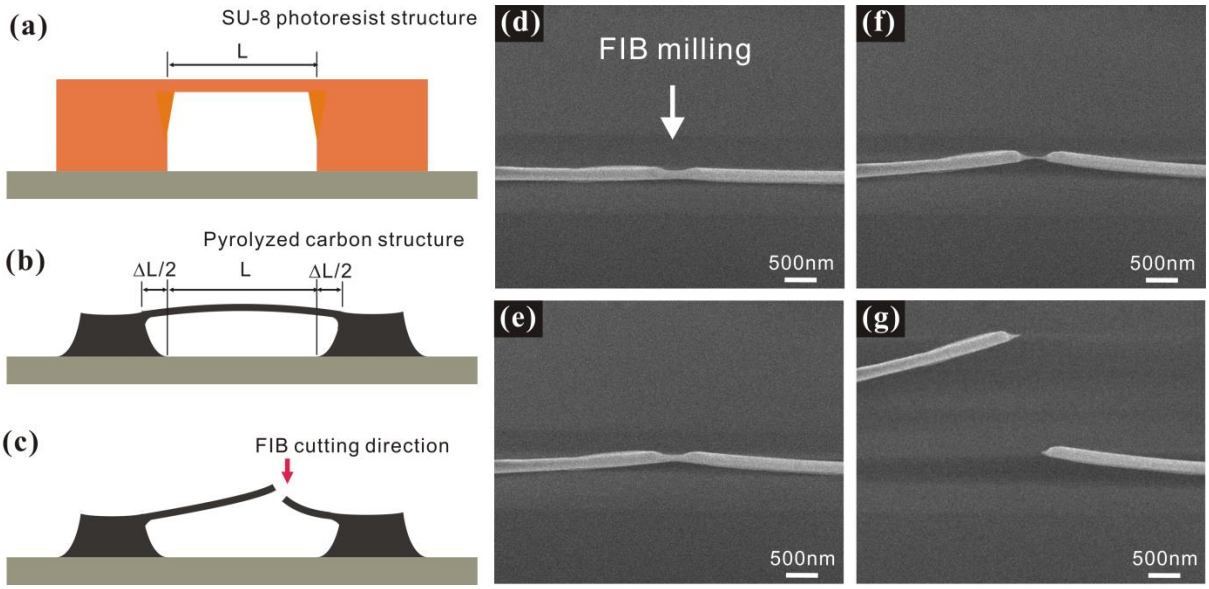

Figure 19. Schematic diagrams of (a) a SU-8 photoresist microwire (b) a carbon nanowire, (b) schematic diagram of a FIB processed suspended carbon nanowire, and (d)-(g) SEM images of a suspended carbon nanowire as a FIB milling process proceeds.[75]

Another unique feature of carbon structure fabrication through C-MEMS is that the electrical properties of carbon are tuned by the pyrolysis temperature [80]. Therefore, it can be manufactured by adjusting the electrical conductivity according to the use purpose of the carbon structure. Figure 20 shows the change in the electrical conductivity of carbon with pyrolysis temperature. In this study, suspended carbon nanomesh is used as structural support for sensor platform and electrical signals are analyzed through ZnO NWs. Therefore, pyrolysis temperature is increased to 700°C to produce relatively low conductivity carbon.

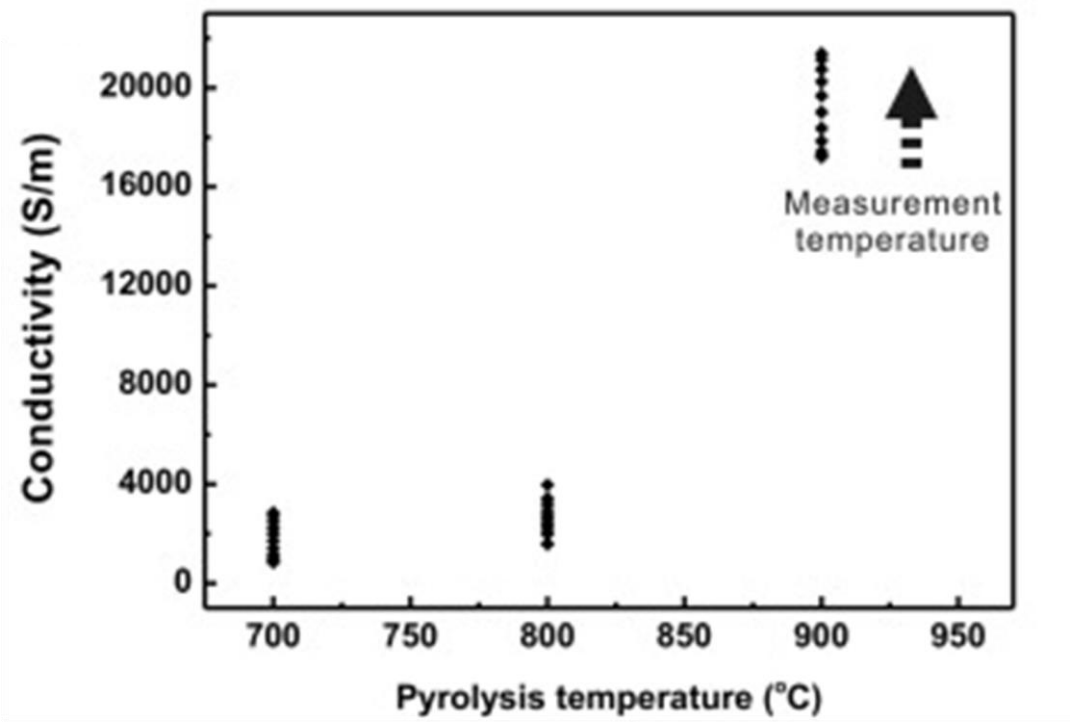

Figure 20. The variation of the electrical conductivity of the carbon pyrolyzed at 700, 800, and 900 ºC (measured temperatures range : from 25 to 200 ºC)[80]

2.3 Hydrothermal synthesis of ZnO NWs

A 7 μm-thick photoresist (AZ4330, AZ Electronic Materials, USA) was spin-coated to patterning the ZnO sputter seed layer. UV exposures were taken a small amount to the top of the coated photoresist to remove only the photoresist around the suspended carbon nanomesh, leaving a photoresist layer on the bottom below the suspended carbon nanomesh. As a result, it is possible to selectively integrate the ZnO seeds only onto the suspended mesh part excluding post. ZnO seeds were deposited using an RF sputtering system (SRN-120, Sorona Co., Ltd, Korea), and the lift-off process was performed using acetone. ZnO nanowires (NWs) were grown by the hydrothermal method. The ZnO hydrothermal method selectively grows ZnO NWs only in the part where the ZnO seed layer is present.

The solution was distilled water in 10 mM concentration of zinc nitrate hexahydrate ($Zn(NO_3)_2 \cdot 6H_2O$, Sigma-aldrich, USA) and 10 mM of hexamethylenetetramine (HMTA, $(CH_2)_6N_4$, Sigma-aldrich, USA). The growth process was conducted in a Teflon/Autoclave container to ensure complete sealing. The container was heated in an oven at 95 ° C for 20 hours to grow ZnO NWs.

2.4 Experimental setup and apparatus

Characterization

The structural and material analysis of the hydrothermally grown ZnO NWs was characterized with scanning electron microscopy (SEM; Quanta 200, FEI company, USA), high-resolution X-ray diffraction (XRD; D8 Advance, Bruker, USA) and transmission electron microscopy (TEM; JEM-2100, JEOL, Ltd., Japan). For the preparation of the TEM sample, a focused-ion-beam milling machine (FIB; Helios 450HP, FEI company, USA) is used.

Gas sensing

A gas sensing setup including a sensing chamber, mass flow controller and source meter is illustrated in Figure 21. The 4 probes are used to contact each electrode of the gas sensor. The ceramic heater is a sample stage so that it can heat up the gas sensor while the sensing test is running. The gas inlet and outlet are on the side walls of the gas sensing chamber and the total inner volume of the sensing chamber is 50ml. Before the target gas flowing, the chamber was purged with several vacuum and N_2 flow cycles to set the stable baseline of the sensing signal. Target gas concentrations were controlled by mass flow controller (MFC; GMC1200, Atovac, Korea) by mixing the target gas with high purity (99.999%) Air or N2 gas. While the gas sensing process, the chamber environment is set to room

temperature, ~40% humidity level, and atmospheric pressure. The resistance change of the sensor was measured by a source meter (KEITHLEY2401, Keithley Instruments, Inc., USA).

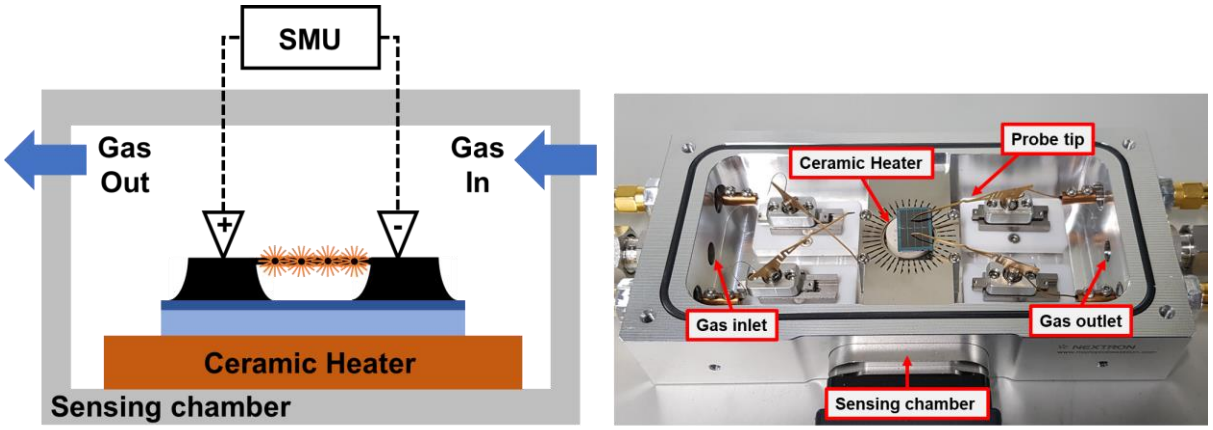

Figure 21. Schematic of gas sensing experiment setup. (a) schematic of sensing chamber (b) real image of inside of the sensing chamber

3 Results and discussion

3.1 Morphology

3.1.1 The suspended carbon nanomesh

The suspended carbon nanomesh structure is fabricated by UV lithography and pyrolysis. The shape of a carbon nanomesh structure is the structure of a contraction of polymer micromesh made of photoresist. As mentioned earlier, during the pyrolysis process, the polymer structure has a volume reduction of 40% to 97% depending on its shape and size [81,82]. As shown in Figure 22, the photoresist structure, suspended polymer micromesh, is isometrically shrunk except for the part attached to the bottom substrate. In particular, in the suspended mesh portion, as shown in (c) and (d) in the width Figure 22, both posts supporting the suspended mesh structure are contracted while pulling the mesh on both sides. As a result, the width of the mesh structure is 20% elongated to 100um to 120um during the pyrolysis. This feature allows the suspended structure to maintain a suspended structure without bending down due to the tensional stress resulting from the contraction of both posts during the pyrolysis process [75,80]. The volume change of the suspended mesh part can be examined in more detail through (e) and (f) in Figure 22. Mesh line width shrinks from 1 um to 300 nm, and the thickness is reduced from 4 um to 400 nm, so the volume reduction of the suspended mesh part is almost 97% high. The height of the suspended carbon nanomesh depends on the height of the photoresist used to fabricate the structure. In this study, SU-8 2025 photoresist was used as a precursor and the height of the photoresist post before pyrolysis was 25 μm. After Pyrolysis, the thickness of the pyrolyzed carbon post was about 11 μm high at the pointed peak and about 8 μm high at the flat part. During the volume reduction of the post, because the shrinkage of the bottom part was limited as it attached to the substrate,

it showed a smaller volume reduction than the suspended mesh part.

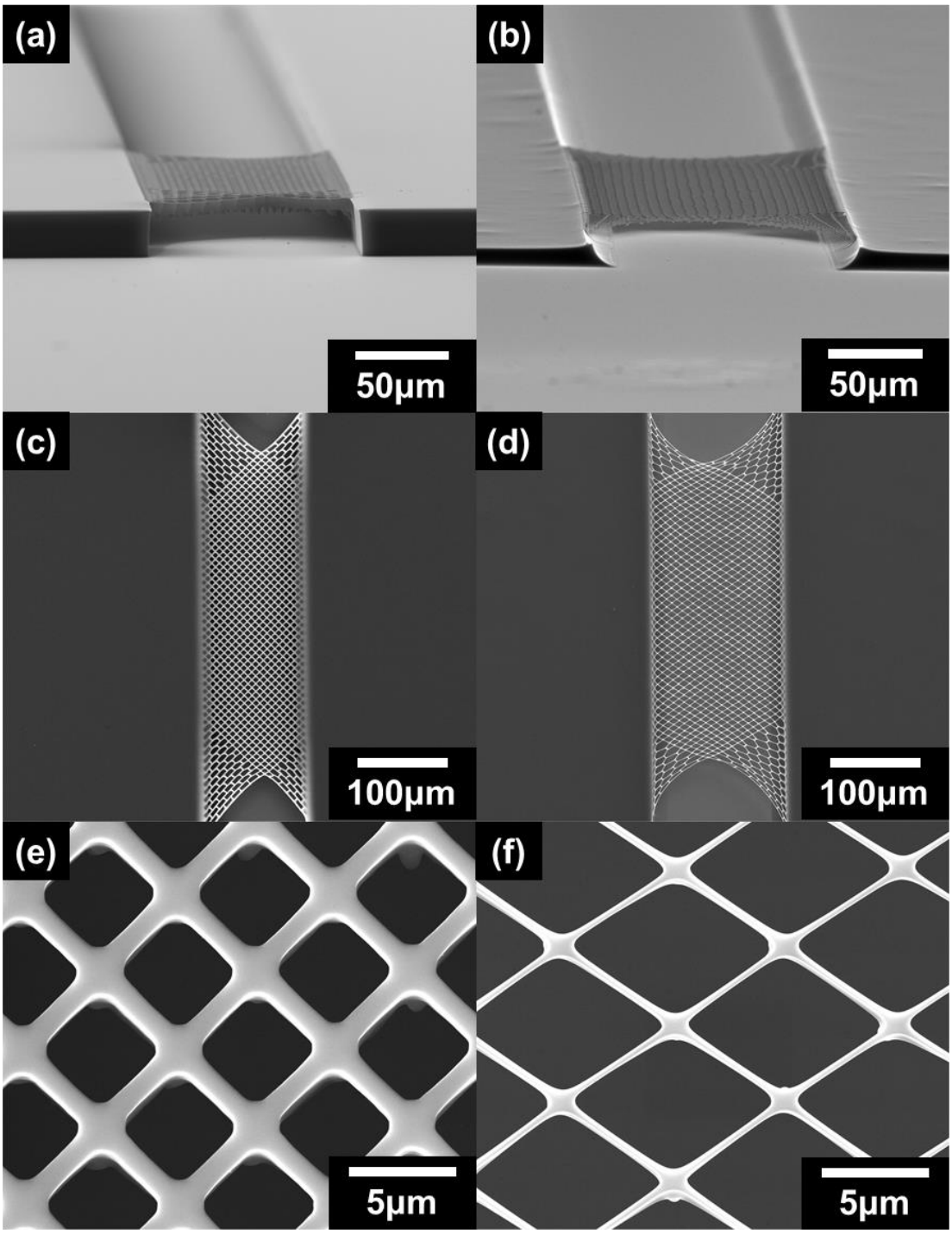

Figure 22. SEM images of (a,c,e) the suspended polymer micromesh before pyrolysis and (b,d,f) the suspended carbon nanomesh after pyrolysis. (a) bird-eye view of the suspended polymer micromesh (b) bird-eye view of the suspended carbon nanomesh (c) top view of the suspended polymer micromesh (d) top view of the suspended carbon nanomesh (e) magnified image of the suspended polymer micromesh

nodes (f) magnified image of the suspended carbon nanomesh nodes.

3.1.2 ZnO NWs

The ZnO NWs are hydrothermally synthesized onto the surface of the suspended carbon nanomesh selectively by depositing the ZnO seed layer only onto the mesh part that is suspended. Figure 23 shows before and after ZnO NWs growth on the suspended carbon nanomesh. As shown in Figure 23, (a) and (b), the ZnO NWs are only grown on the suspended mesh part and the side posts surface is kept clean. Therefore, it is reasonable to assume that most of the electrical signal variation of the gas sensor is from the ZnO NWs. The shapes of the voids of the mesh filled with ZnO NWs junctions can be confirmed through (c) and (d) in Figure 23. These ZnO NWs junctions form a network across the mesh and connect both posts. The (e) and (f) in Figure 23 show the ZnO growth profile at the mesh one node. ZnO having a diameter of 30 to 70 nm and a length of 2.5 to 3.5 μm are densely grown.

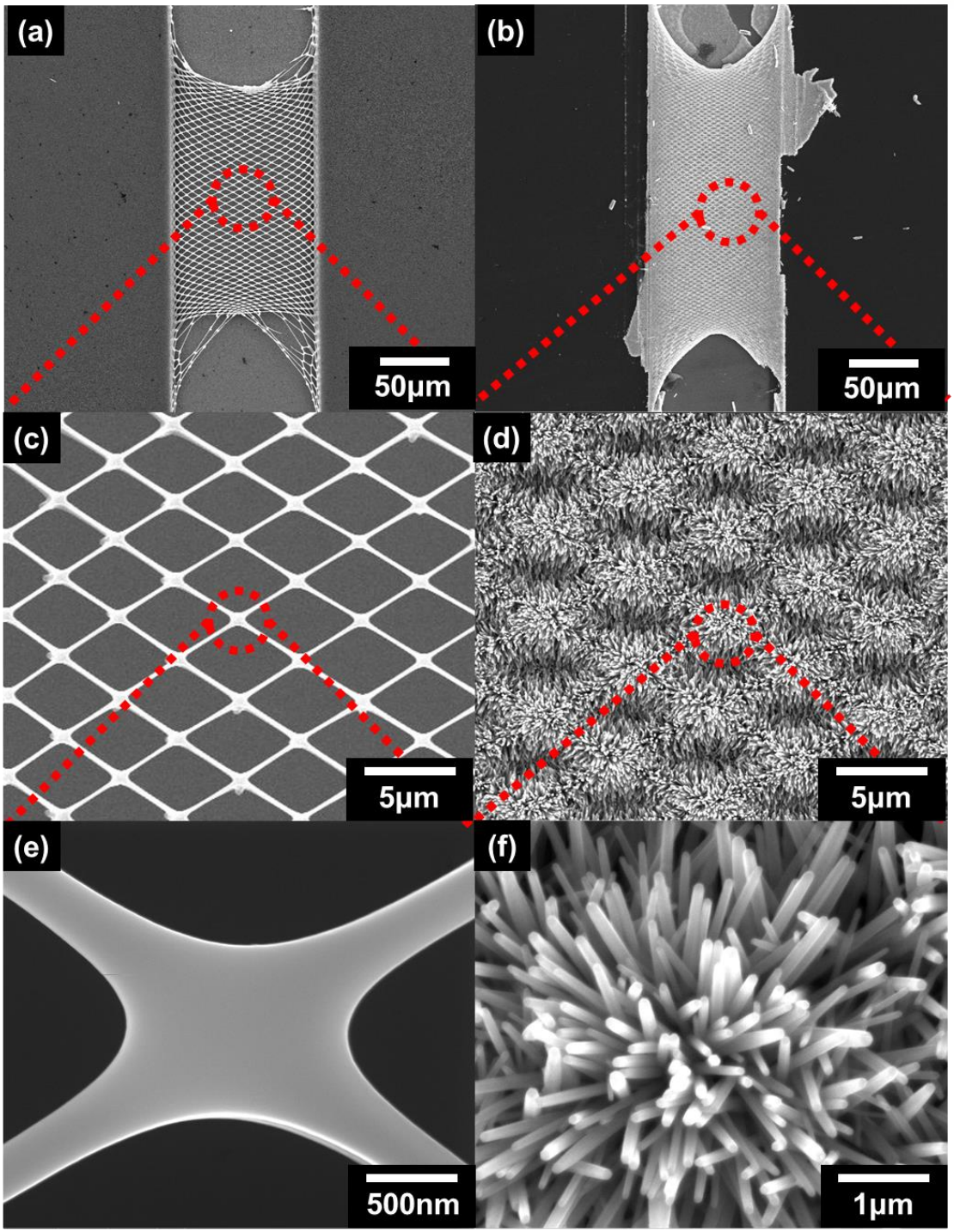

Figure 23. SEM images of (a,c,e) the bare suspended carbon nanomesh before hydrothermal process and (b,d,f) the suspended carbon nanomesh functionalized with ZnO NWs. (a) top view of the bare suspended carbon nanomesh (b) top view of the suspended carbon nanomesh functionalized with ZnO NWs (c) magnified carbon mesh part (d) magnified carbon mesh functionalized with ZnO NWs (e) one node of the carbon nanomesh (f) one node of the carbon nanomesh functionalized with ZnO NWs

The crystal structures of ZnO NWs were analyzed by HR-TEM and XRD and are shown in Figures 24 and 25, respectively. For TEM analysis, the sample was prepared with a flat carbon pad and then ZnO NWs grown on that pad. As shown in Figure 24, the HR-TEM image shows the interplane section of carbon/ZnO seed/ZnO NWs structure. Magnetized image of single ZnO NW (b) showed high crystallinity with corresponding diffraction pattern (c) and inverse FFT image (d). The inverse FFT images showed 0.026 nm spacing which corresponds to the spacing of the ZnO crystal lattice conforming that grown ZnO NWs are highly crystallized [83].

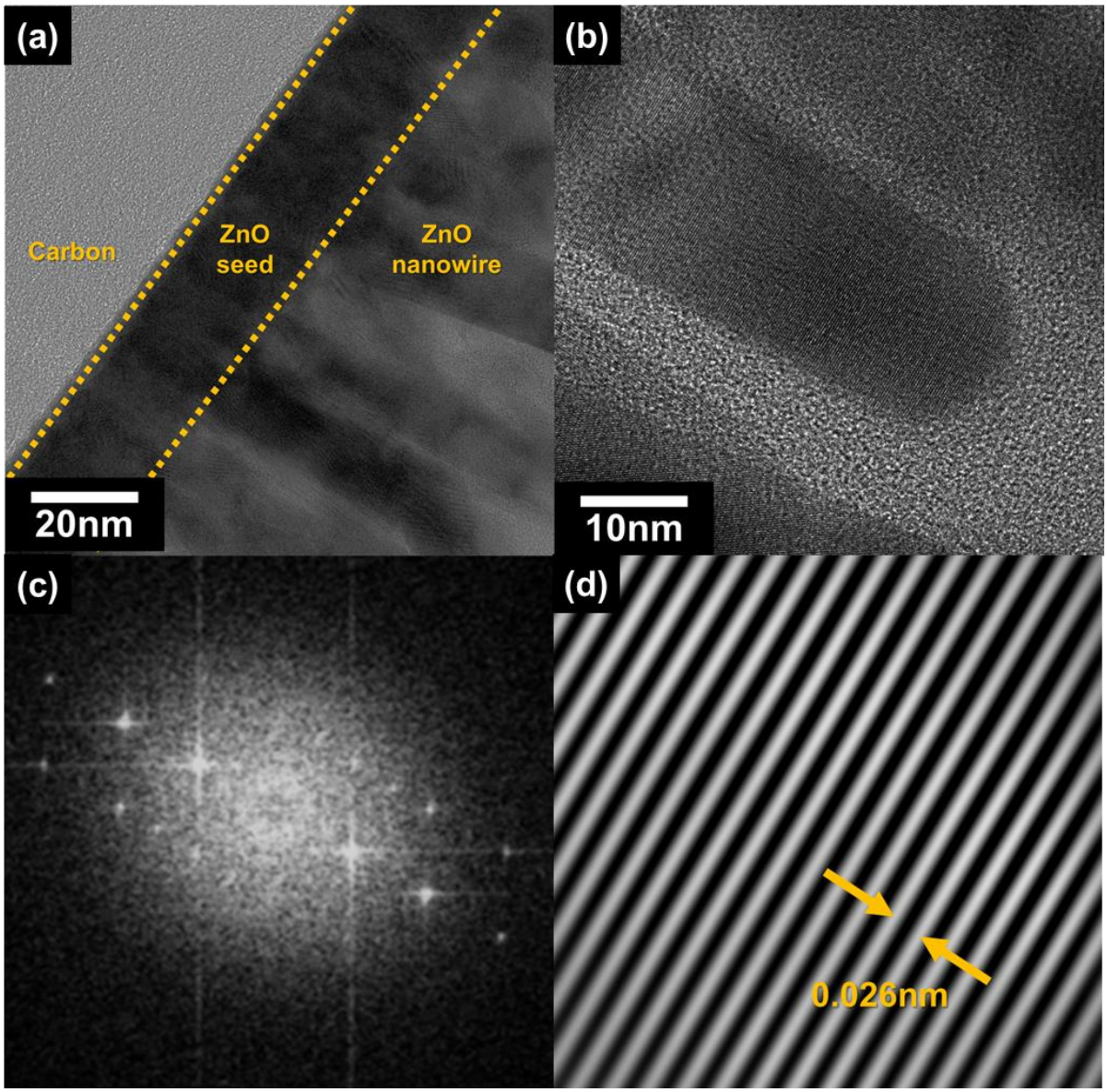

Figure 24. TEM results of synthesized ZnO nanowires: (a) TEM image of the prepared sample structure at the boundaries. (b) TEM image of the one ZnO nanowire tip. (c) corresponding diffraction pattern of ZnO nanowire. (d) corresponding inverse FFT image of ZnO nanowire.

For XRD analysis, the sample was prepared on the quartz wafer to avoid the Si peak. On the quartz wafer, a thin carbon film is fabricated and the ZnO NWs were integrated on to that carbon film surface using the same process of sensor fabrication. As shown in Figure 25, there is a high (002) peak which indicates wire-like growth direction of the synthesized ZnO nanostructure since (002) plane is the top surface of hexagonal prism ZnO crystal [84]. So, it confirms that ZnO nanostructure is 1-D

nanowire with a high aspect ratio. A rough peak around 20~30 degree was originated from carbon and quartz substrate.

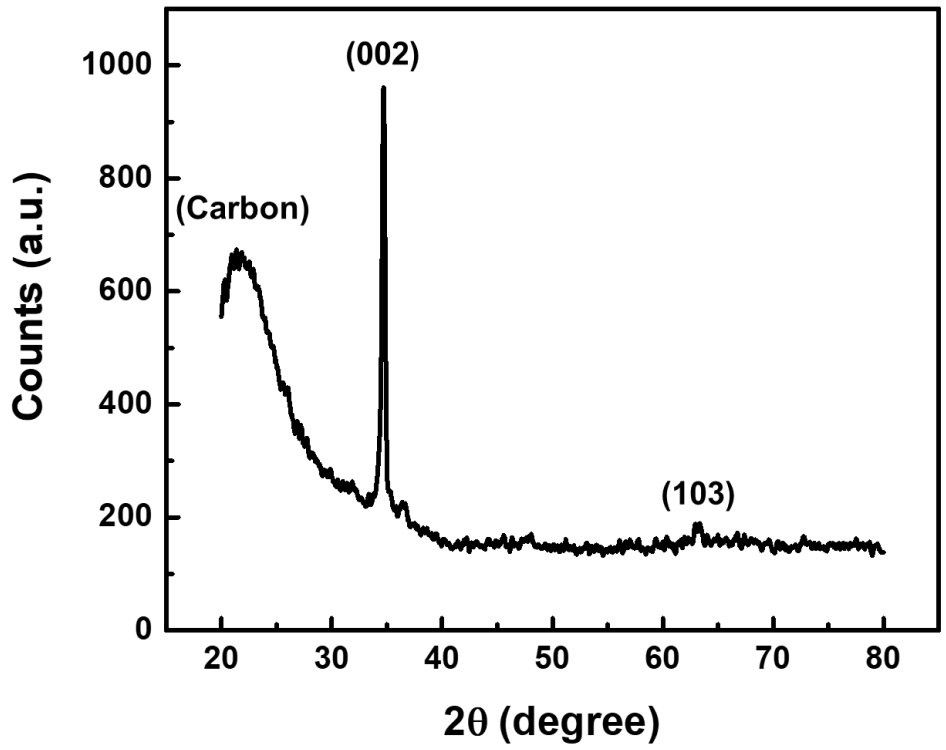

Figure 25 HRXRD pattern of ZnO NWs grown on a pyrolyzed carbon thin film.

The electrical characteristics of the proposed gas sensor were analyzed by the I-V curve. All electrical connections are stable, as shown in Figure 26. It can be seen that the electrical resistance difference between the carbon structure and the ZnO part is not so large at room temperature. However, at 300 ℃, the conductivity of ZnO increases greatly [85], so the total resistance of the sensor is greatly reduced. At this temperature, as shown in (b), the resistance difference between the carbon structure and the ZnO part becomes very large. Since the proposed sensor operates at high temperature, the change of resistance obtained from the gas sensor can be regarded as the resistance change of the only

ZnO part even though there is no insulation layer separating carbon and ZnO portions.

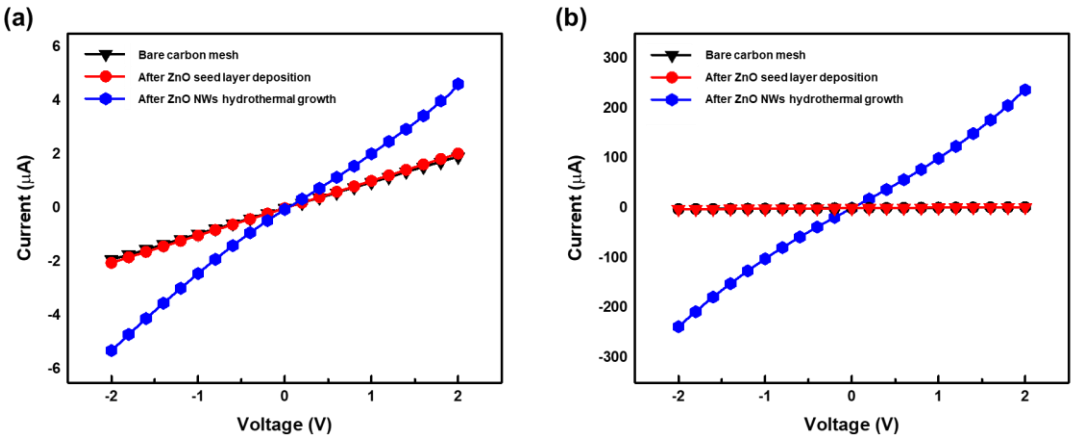

Figure 26 I-V curve of a bare suspended carbon nanomesh(black line), after ZnO seed layer deposition(red line) and after ZnO NWs hydrothermal growth(blue line) at the temperature of (a)27℃ and (b)300℃

3.1.3 ZnO NWs junction structure

Confirmation of the junction formation of ZnO NWs was confirmed by SEM images. As shown in Figure 27, the ZnO NW was radially distributed surrounding the elliptical carbon backbone structure. These ZnO NWs were grown from each mesh line and were found to meet each other forming a junction. Since the length of ZnO NW is long enough to be 2.5 ~ 3.5 μm, the junction could be formed across the mesh's empty spacings. Since the diameter of ZnO NWs is as thin as 30nm ~ 70nm, it is confirmed that a large number of ZnO NWs surround one mesh line forming dense ZnO NWs junctions. The morphology of grown ZnO NWs was uniform as shown in Figure 27.

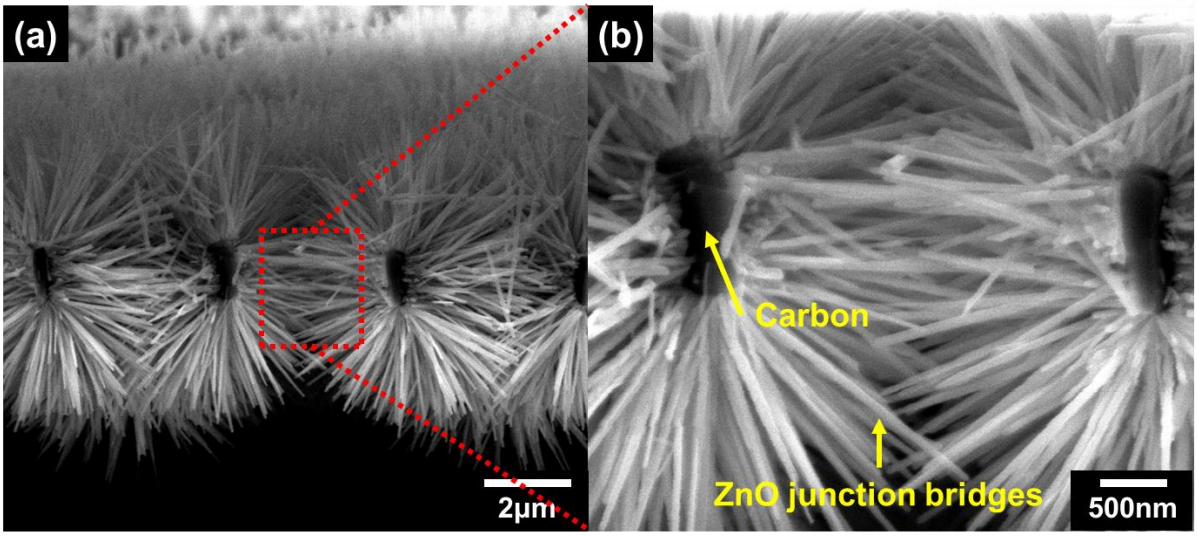

Figure 27. Section view of the suspended carbon nanomesh functionalized with ZnO nanowires

The EDS analysis was conducted based on the SEM image. The components of ZnO NW and carbon nanomesh were quantitatively analyzed. As shown in Figure 28, the elements other than Zn and O are not visible on the ZnO NW, and the elements of C are greatly increased in the carbon nanomesh part. The peaks for the other elements were insignificant, confirming that there were no unwanted impurities.

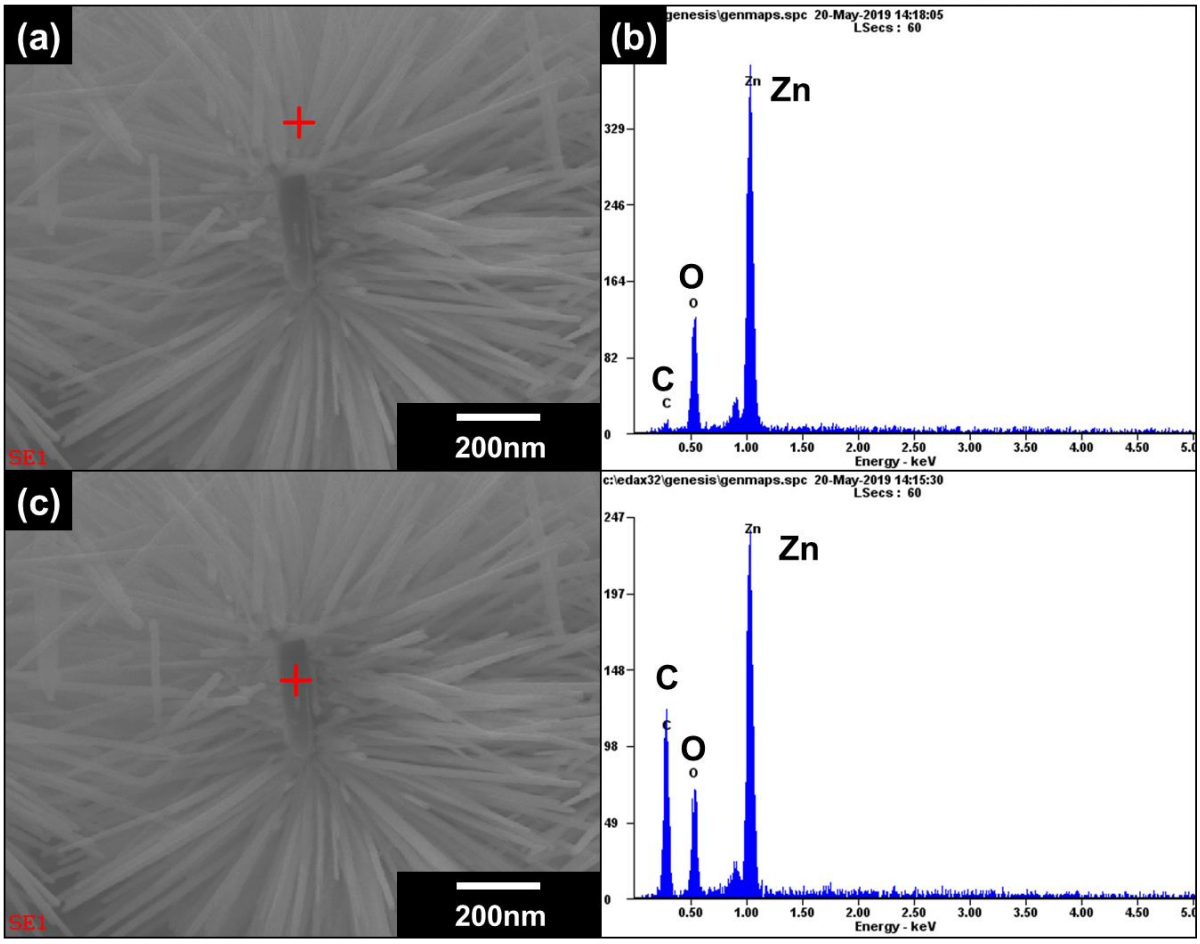

Figure 28. EDS analysis of the suspended carbon nanomesh functionalized with ZnO NWs (a) point EDS on the ZnO NWs (b) point EDS on the carbon nanomesh.

3.2 Sensor optimization

3.2.1 Working temperature

The analysis of the temperature operating condition of the gas sensor was carried out. The performance of metal oxide-based gas sensors is strongly affected by temperature [7,9]. Therefore, in order to analyze the optimal operating temperature of the sensor proposed in this study, the performance of the sensor was evaluated by varying the temperature of the ceramic heater in the sensing chamber. The performance evaluation of the sensor was performed at intervals of 25°C from 200°C to 325°C. For

all temperature conditions, 5 ppm NO_2 gas was injected for 5 minutes and sensor response was recovered by N_2 gas for 10 minutes. As shown in Figure 29, the response of the sensor rapidly increases from 200°C to 275°C, after which it begins to decrease again. The magnitude of the sensor response was the largest at 275°C (~647). We also evaluated the response and recovery times. The response time was steadily reduced from 200°C to 300°C, which showed the fastest response time at 300°C but slowed down again at 325°C. Recovery time tended to decrease steadily as the temperature increased from 275°C to 325°C. Considering the magnitude of response, response time, and recovery time, it is concluded that the sensor performance at 275 ~ 300°C is most desirable. All subsequent analyses were performed at 275°C, where the response was the largest and showed a reasonable response time and recovery time.

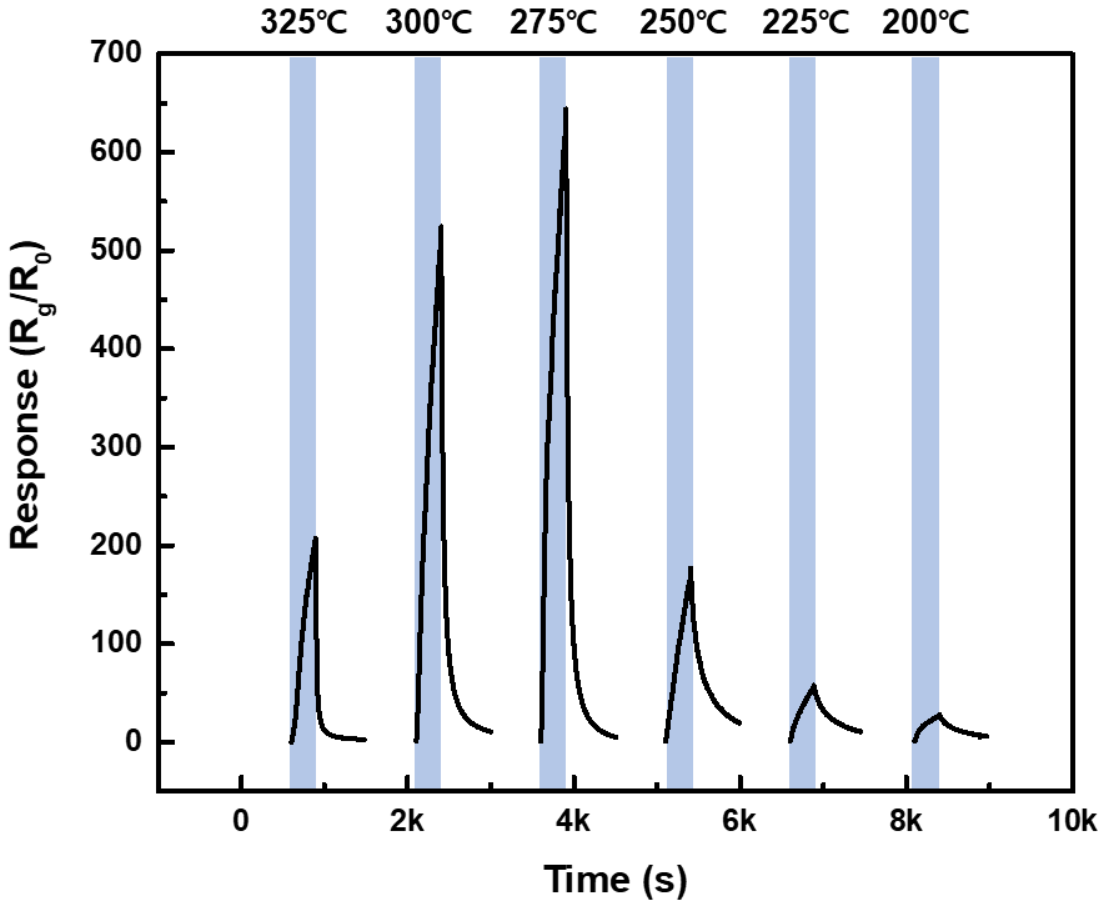

Figure 29 Sensor response to 5ppm NO_2 gas according to working temperature from 200°C to 325°C.

3.2.2 ZnO NWs morphology control

The aspect ratio of ZnO NW was compared and analyzed. The morphology of ZnO NWs grown by hydrothermal growth can be tuned through hydrothermal conditions such as solution concentration and time [86-88]. As described above, the ZnO based gas sensor is based on the relative thickness variation of the conducting channel inside the ZnO crystal and the electron depletion layer of the surface. Therefore, in the case of ZnO NW, the sensing performance varies depending on the diameter. In order to compare the performance of ZnO NWs according to the diameter of the sensor

presented in this study, the chemical concentration of the hydrothermal solution was changed to 10mM / 25mM / 35mM. The results shown in Figure 30 are the results when grown to 25mM (e,f) 35mM at 10mM (c,d) for each (a,b) with the same concentrations of $Zn(NO_3)_2$ and HMTA. The growth time was fixed for 20 hours and the temperature was fixed at 95°C. The average diameter of ZnO NWs synthesized with 10 mM growth solution was 30 ~ 70nm and the length was about 2.5 ~ 3.5um. The average diameter of ZnO NWs synthesized with 25mM growth solution was about 80 ~ 120nm and the length was about 3.5μm. ZnO NWs synthesized with the highest concentration of 35 mM growth solution were about 4-5μm in diameter with a length of about 100-200nm. As shown in Figure 30, the length of the ZnO NW at higher concentration is longer, but the number of NW per unit area decreases as the diameter becomes much thicker. Furthermore, in the case of the 35mM growth solution, the ZnO NWs were too thick to be merged with each other to fill the gap therebetween. As a result, gas access became disadvantageous.

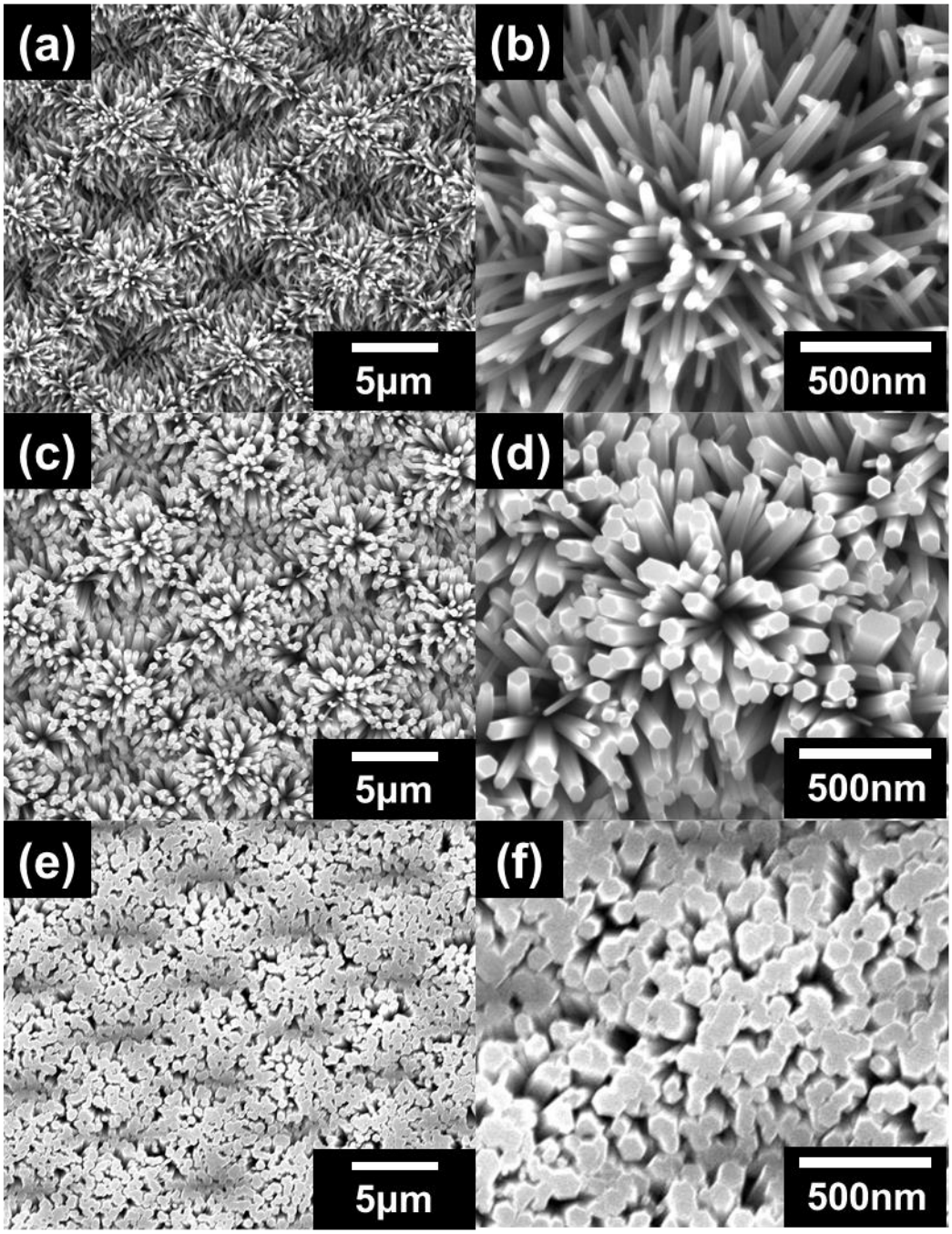

Figure 30. SEM images of hydrothermally grown ZnO NWs on the carbon nanomesh according to concentration of the growth solution. (a,b) ZnO NWs synthesized with 10mM of $Zn(NO_3)_2$ and HTMA (c,d) ZnO NWs synthesized with 25mM of $Zn(NO_3)_2$ and HTMA (e,f) ZnO NWs synthesized with 35mM of $Zn(NO_3)_2$ and HTMA

Gas sensing performance comparisons for ZnO NWs grown under each condition were compared and compared at an operating temperature of 275°C with 5 ppm NO_2 gas. As shown in Figure

31, the response of the sensor decreases as the concentration of the growth solution increases. Therefore, it was confirmed that the thinner the diameter, the more sensitive the sensor becomes in the range of tens ~ hundreds of nm scale. When the concentration of the hydrothermal solution was adjusted to less than 10mM, it failed to grow crystals of uniform ZnO NW type. Therefore, ZnO NW was synthesized on the basis of 10 mM growth solution which showed the best reactivity at the concentration that can grow uniform ZnO NWs.

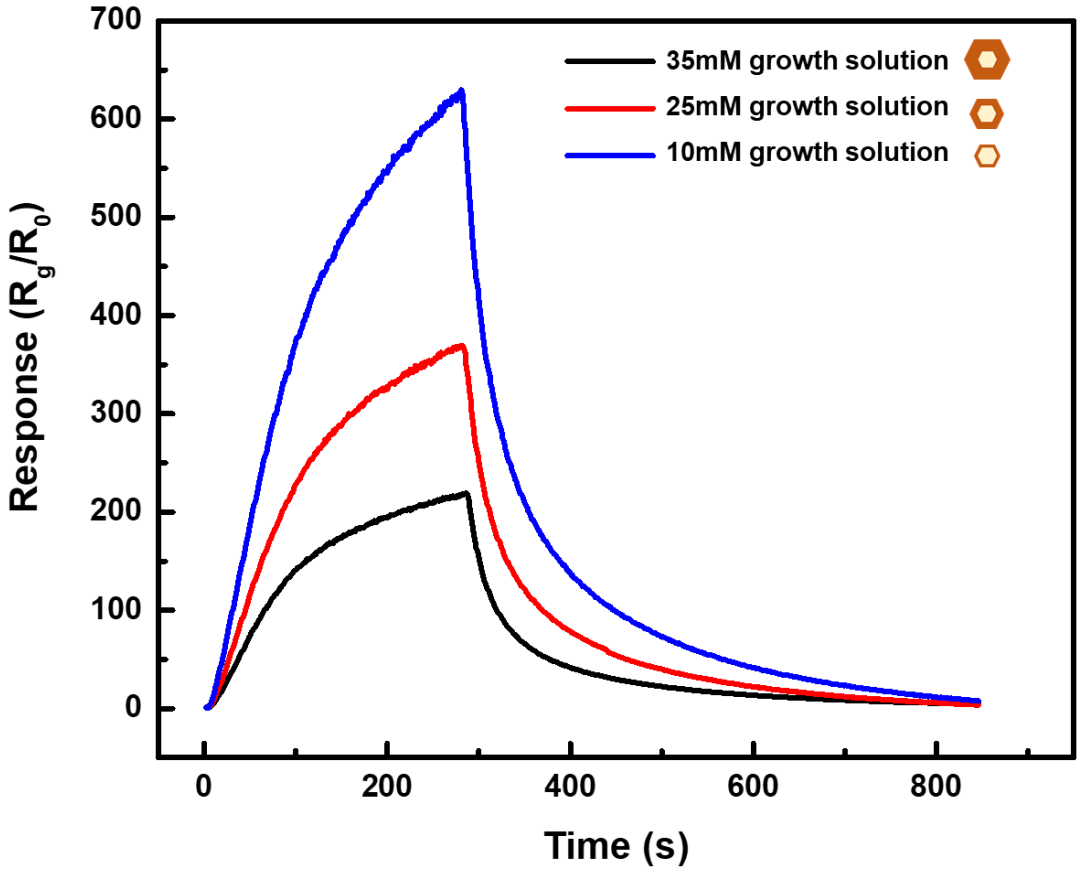

Figure 31. Comparison graph of the gas responses to 5ppm NO_2 gas at 275°C according to concentration of the hydrothermal growth solution.

3.3 Sensor characterization

3.3.1 Effect of the suspended structure

The effect of the suspended structure is analyzed by comparing the suspended and substrate-bound structure. To clearly compare the only suspension property, two samples are prepared as illustrated in Figure 32. Substrate bound carbon mesh and suspended carbon mesh is prepared through the same pyrolysis condition to avoid any other factors which can affect the result. ZnO NWs are also grown in the same condition result in short and thin ZnO NWs (diameter~50nm length~800nm). Since the suspended nature gives more effective mass transfer, the faster reaction speed is expected. Also, by employing a suspended structure, the sensor can be free from the blocking effect by the bottom substrate and stagnant layer formation near the substrate [75,79,89]. These become factors that speed up the reaction and recovery of the gas sensor.

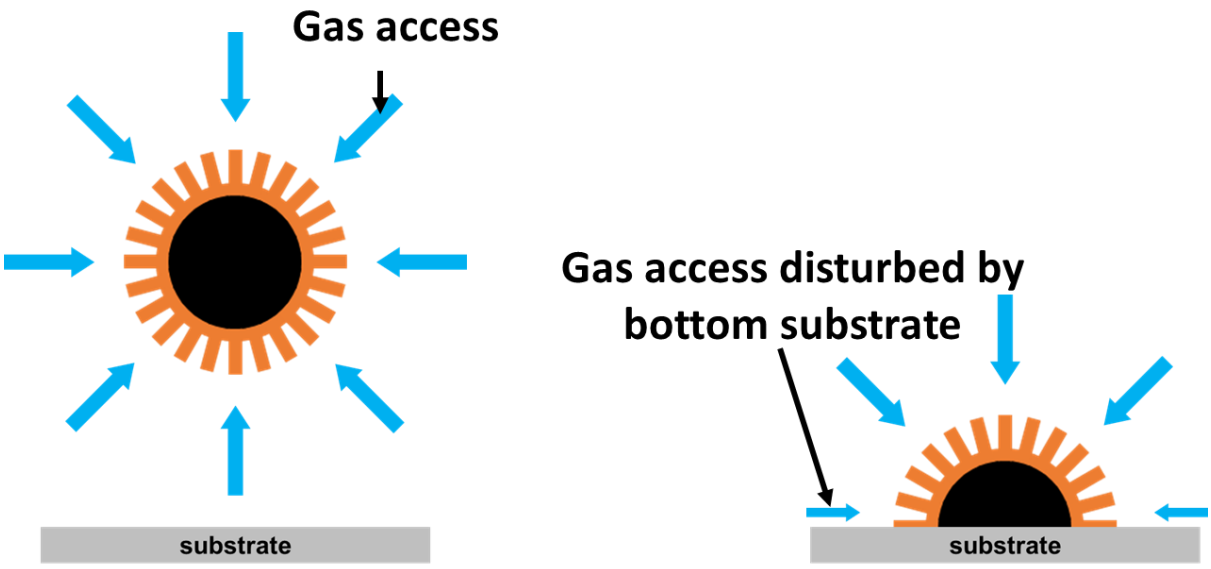

Figure 32. Schematic images of the suspended gas sensor and the substrate-bound gas sensor.

The suspended carbon mesh-based gas sensor and the substrate-bound mesh-based gas sensor are compared with respect to the 5ppm NO2 gas at 275°C. As shown in Figure 33, the suspended one

showed not only higher response but also a faster reaction speed. The response of the suspended structure is much higher than the substrate-bound mesh of about 330 to 180. Furthermore, the response time of the suspended structure was 204 seconds, faster than the substrate bound of 281 s, and the recovery time was much faster than the suspended structure of 303 seconds and the substrate-bound of 420 seconds. By adopting a structurally suspended type in the design of the gas sensor, advantages in terms of the sensitivity and the reaction speed are expected.

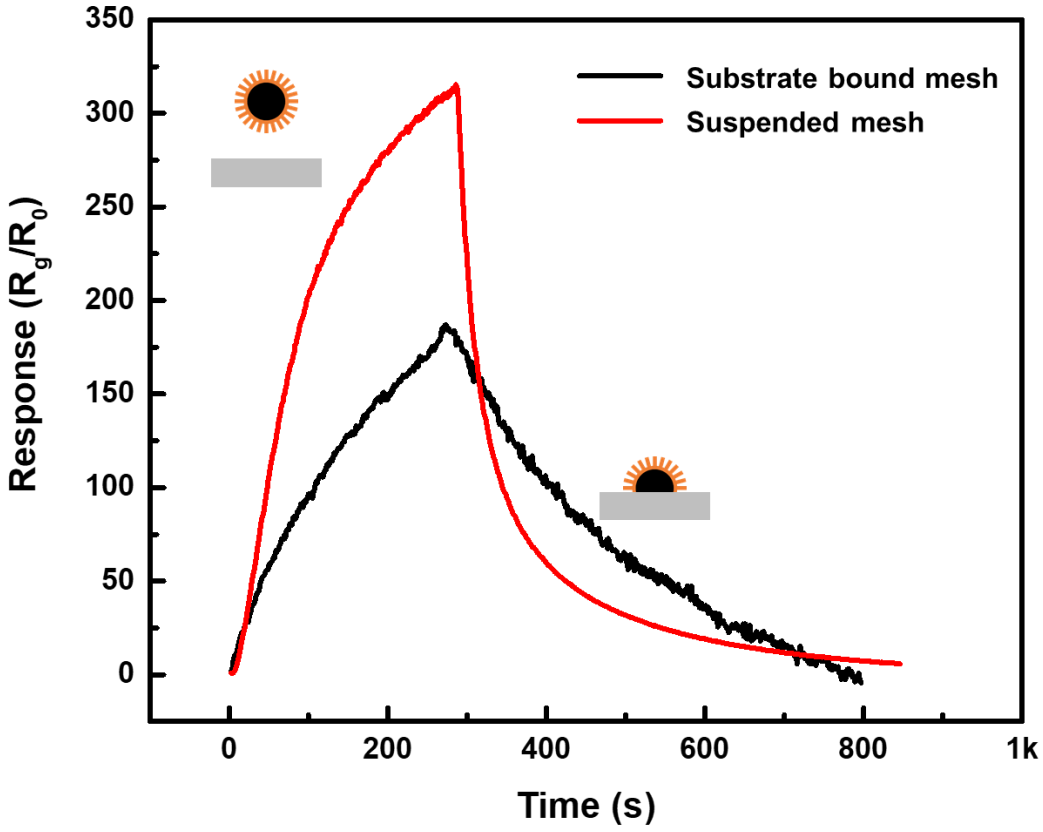

Figure 33. Comparison graph of the response of the substrate bound mesh and the suspended mesh under 5ppm NO_2 at 275°C. inset images are schematic images of structure of each sensor

3.3.2 Effect of the ZnO NWs junction structure

The effect of junction structure on sensor performance was analyzed. As shown in Figure 34, metal oxide junctions are formed to provide an additional current path to the sensor. Since a potential barrier is formed at the junction of the metal oxide, a certain level of energy is required to flow electrons over these junction barriers. This potential barrier's level also changes as the metal oxide reacts with the reducing or oxidizing gases. This results in an additional gas sensing mechanism based on potential barriers [77,78,90]. As a result, two different mechanisms simultaneously act on the 'change in the thickness of the electron depletion layer of the metal oxide nanowire itself' and the 'change in the potential barrier in the metal oxide junction', enabling gas detection for a wider range of concentrations. In addition, since the number of factors influencing the electron flow increases for the same gas condition, the number of flowing electrons also increased more greatly. This means that the structure with metal oxide junctions can have a higher response than the structure without it.

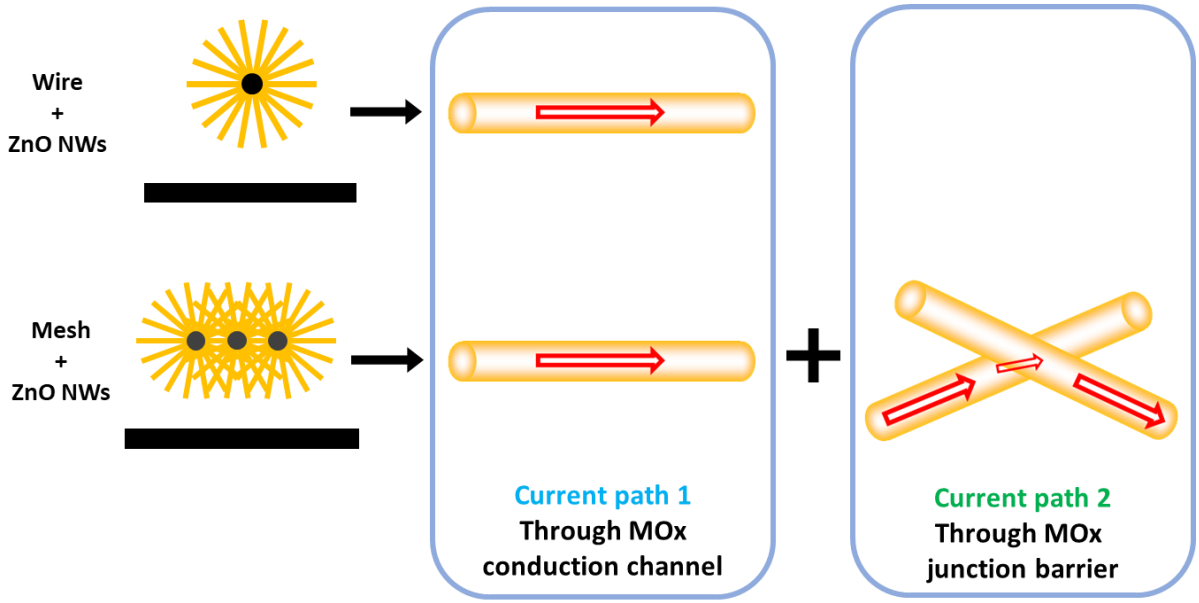

Figure 34. Schematic images of comparison between ZnO integrated onto the wire and onto the mesh.

In this study, three models were constructed to compare the effects of ZnO junctions. As shown

in Figure 35, single wire and short ZnO NWs, mesh and short ZnO NWs, mesh and long ZnO NWs were fabricated. First, in the case of the short ZnO NWs integrated on the suspended carbon nanowire shown in Figure 35 (a), there is almost no ZnO NWs junction. (b), a small number of ZnO NWs junctions are formed at nodes where mesh lines intersect. (c), the junctions are formed much more because the ZnO NWs are sufficiently long enough to form junctions across the mesh spacing.

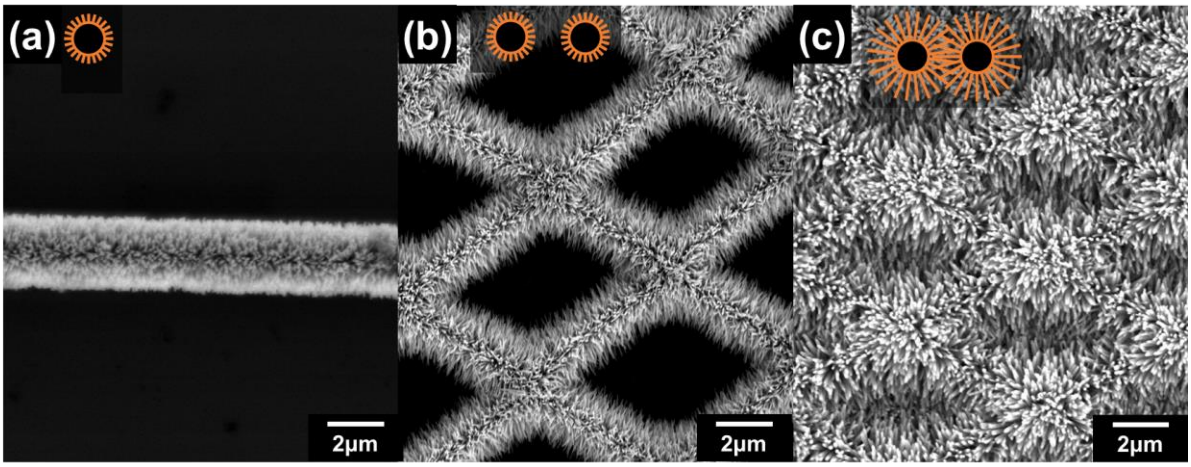

Figure 35. SEM images of (a) short ZnO NWs integrated on the suspended carbon nanowire. (b) short ZnO nanowires integrated on the suspended carbon nanomesh. (c) long ZnO nanowires integrated on the suspended carbon nanomesh. Inset images are schematic images of each structure.

As shown in Figure 36, the structure of the long ZnO NWs / carbon nanomesh where the junction is formed most dense showed the largest sensor response. In the case of a short ZnO NWs / carbon single wire with few junctions, the sensor response suddenly saturates after a concentration of 3 ppm. However, as the junction structure increases, the saturation effect also weakens at the same concentration. Therefore, the sensor could operate reasonably in a wider range of gas concentrations as the number of junctions is larger. The sensitivity of the long ZnO NWs / carbon nanomesh structure with the highest junction was the highest with a sensitivity of 200.59 ppb^{-1}. The short ZnO NWs / carbon mesh and the short ZnO NWs / carbon single wire were 135.08 ppb^{-1} 120.29 ppb^{-1}. (The fitting curve

was calculated from the concentration of 50 ppb to 500 ppb with R^2 value of 0.99). In conclusion, the ZnO NWs junction enhances the sensitivity of the sensor and broadens the sensing range. These effects are shown to be larger as the ZnO NWs junction is more denser.

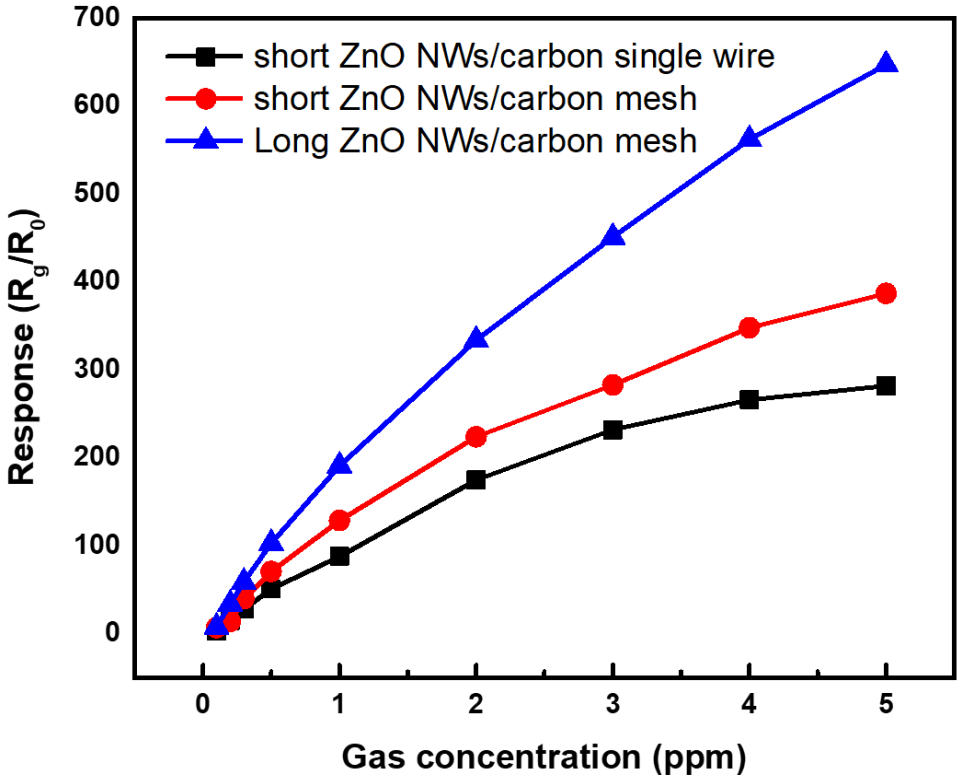

Figure 36. Sensor response comparison graph between short ZnO NWs/single carbon nanowire(black line), short ZnO NWs/carbon nanomesh(red line) and Long ZnO NWs/carbon nanomesh(blue line) to various concentration of NO_2 at 275°C

3.4 Sensor performance

3.4.1 Gas sensing performance

The performance of the proposed gas sensor was measured by resistance change to different concentrations of the target gas. Figure 37 shows the performance of gas sensor based on the suspended

carbon nanomesh functionalized with ZnO NWs and their junction to NO_2 gas concentrations of 50 ppb-5 ppm at 275°C. All concentrations of NO_2 gas were injected for 5 min and N_2 gas was injected for recovery for 10 min. The response of the sensor is expressed as R_g/R_0 (R_g: maximum resistance after target gas injection, R_0: basic resistance before gas reaction). ZnO is an n-type metal oxide, and NO_2 gas acts as an oxidizing gas. Therefore, the NO_2 gas increases the concentration of oxygen molecules adsorbed on the ZnO surface, increasing the electron depletion layer thickness of the ZnO nanostructure, and decreasing the width of the conduction channel. As a result, the resistivity of the ZnO crystal is increased. This makes that the response of the gas sensor to the target gas can be analyzed simply by recording the change in resistance [77,79]. This phenomenon becomes more apparent as the concentration of target gas increases. In this study, the gas sensor based on suspended carbon nanomesh functionalized with ZnO NWs and their junctions shows a very high gas response of 633 to 5 ppm NO_2 gas and a steady increase in gas response within the measurement range of 50 ppb to 5 ppm indicating that it can detect a wider range of gases.

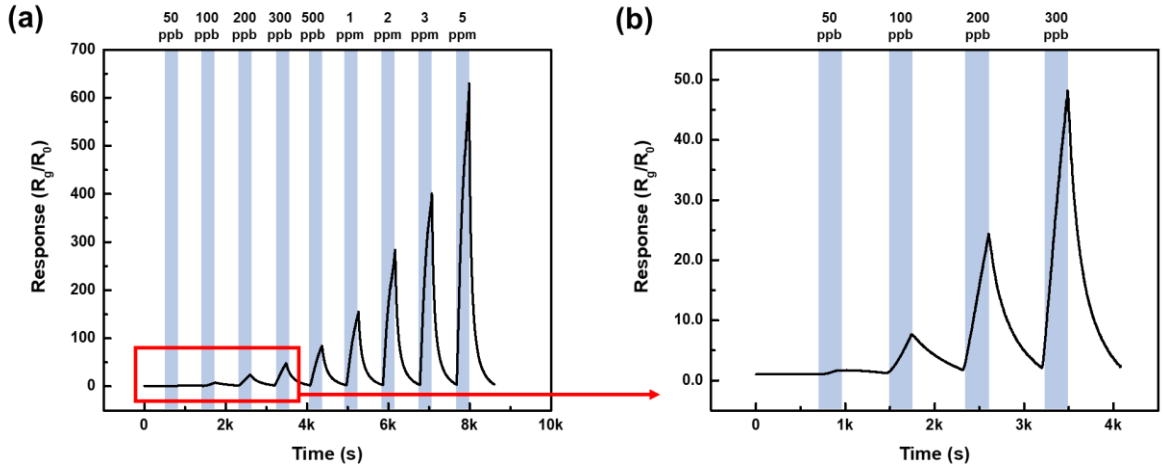

Figure 37. Gas sensing graph of the suspended carbon nanomesh functionalized with ZnO nanowires to various concentration of NO_2 gas ranging from (a)50 ppb to 5 ppm at 275°C (b) 50 ppb to 300 ppb.

So far, most of the sensor characterizations were conducted based on the NO_2 gas due to the highest reactivity to ZnO material. Gas sensing performances of some other gases are analyzed below.

As illustrated in Figure 38, the sensor performance to C_6H_6 gas ranging from 2 ppm to 600 ppm was analyzed under the temperature of 275°C. The concentration of C_6H_6 is controlled by mixing dry air by MFC. The gas response to C_6H_6 gas increases linearly from 2 ppm to 400 ppm. Above the 400 ppm C_6H_6 concentration range, the gas response was gradually saturated.

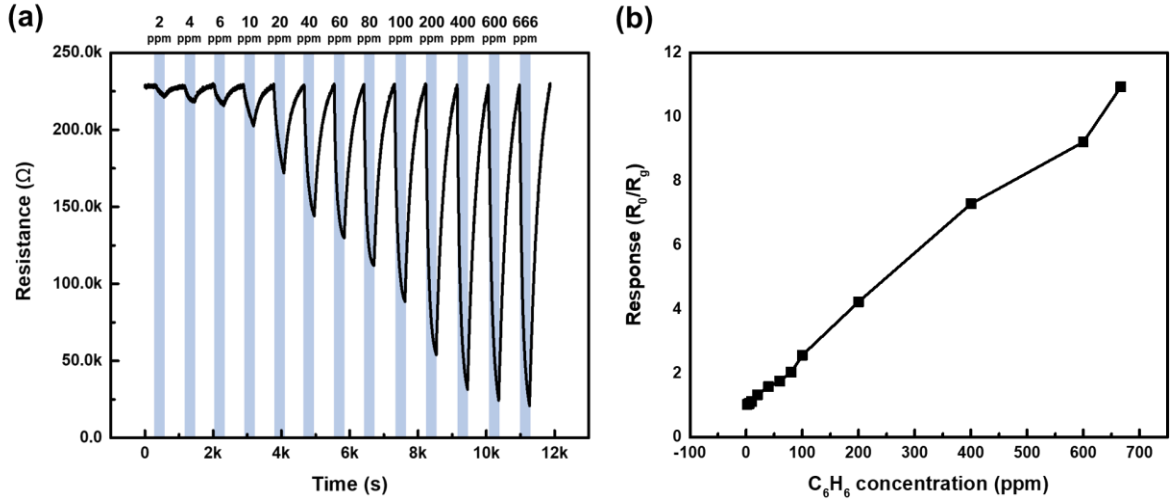

Figure 38. Gas sensing performance of the suspended carbon nanomesh functionalized with ZnO nanowires to various concentration of C_6H_6 gas ranging from 2 ppm to 666 ppm at 275°C (a) resistance change under various concentration of C_6H_6 (b) corresponding response versus C_6H_6 concentration.

As illustrated in figure 39, the sensor performance to CH_4 gas ranging from 50 ppm to 1 % was analyzed under the temperature of 275°C. The concentration of CH_4 is controlled by mixing dry air by MFC. The gas response to CH_4 gas increases linearly from 50 ppm to 0.1 %. Above the 0.1% CH_4 concentration range, the gas response was gradually saturated.

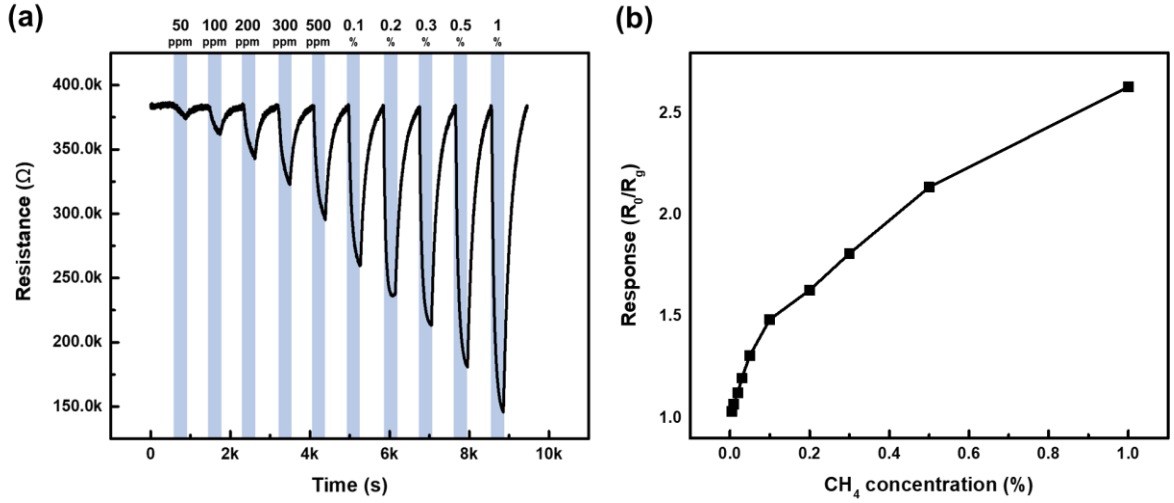

Figure 39. Gas sensing performance of the suspended carbon nanomesh functionalized with ZnO nanowires to various concentration of CH_4 gas ranging from 50 ppm to 1 % at 275ºC (a) resistance change under various concentration of CH_4 (b) corresponding response versus CH_4 concentration.

As illustrated in figure 40, the sensor performance to CO gas ranging from 50 ppb to 33 ppm was analyzed under the temperature of 275ºC. The concentration of CO is controlled by mixing dry air by MFC. The gas response to CO gas increases linearly from 50 ppb to 5 ppm. Above the 5ppm CO concentration range, the gas response was gradually saturated.

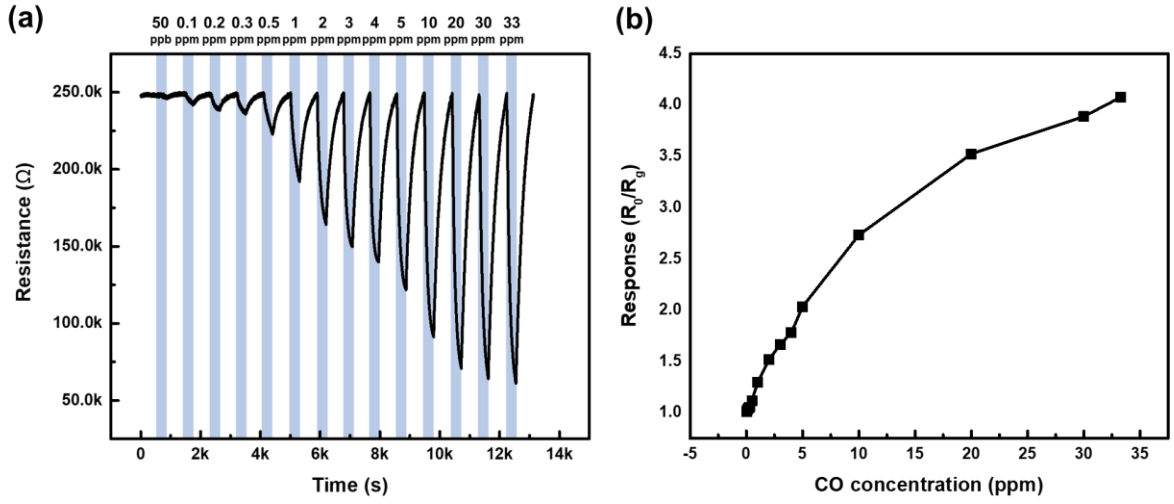

Figure 40. Gas sensing performance of the suspended carbon nanomesh functionalized with ZnO

nanowires to various concentration of CO gas ranging from 50 ppb to 33ppm at 275°C (a) resistance change under various concentration of CO (b) corresponding response versus CO concentration.

As illustrated in figure 41, the sensor performance to H_2 gas ranging from 0.5 ppm to 333 ppm was analyzed under the temperature of 275°C. The concentration of H_2 is controlled by mixing dry air by MFC. The gas response to H_2 gas increases linearly from 0.5 ppm to 50 ppm. Above the 0.5 ppm H_2 concentration range, the gas response was saturated.

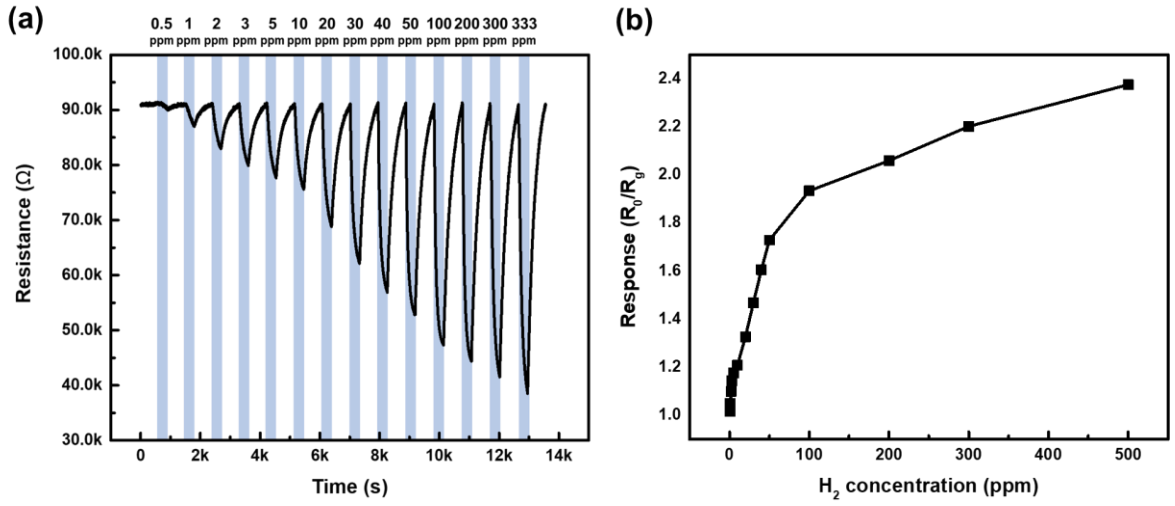

Figure 41. Gas sensing performance of the suspended carbon nanomesh functionalized with ZnO nanowires to various concentration of H_2 gas ranging from 0.5 ppm to 333ppm at 275°C (a) resistance change under various concentration of H_2 (b) corresponding response versus H_2 concentration.

As illustrated in Figure 42, the sensor performance to SO_2 gas ranging from 50 ppb to 33 ppm was analyzed under the temperature of 275°C. The concentration of SO_2 is controlled by mixing dry air by MFC. The gas response to SO_2 gas increases linearly from 50 ppb to 5 ppm. Above the 5 ppm SO_2 concentration range, the gas response was saturated.

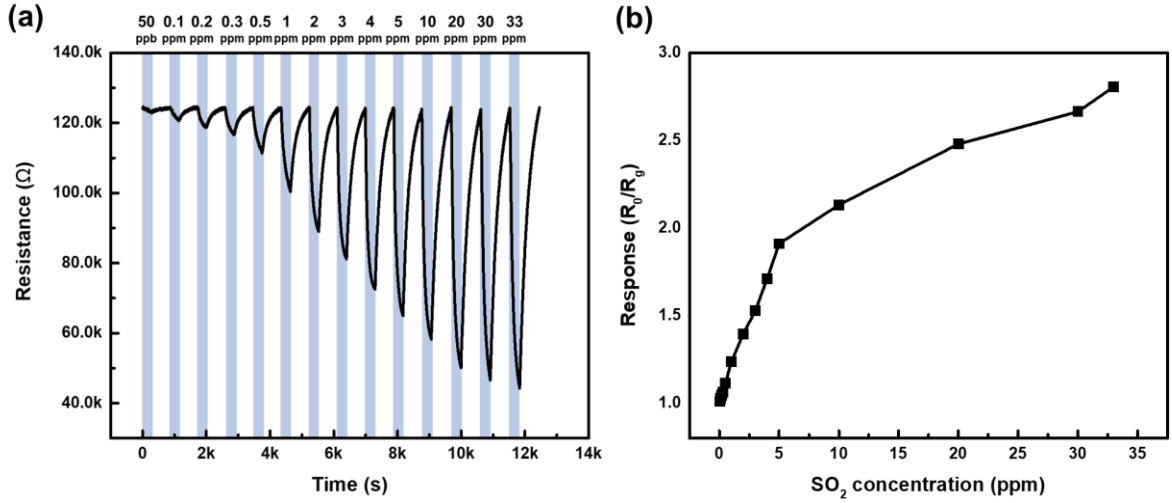

Figure 42. Gas sensing performance of the suspended carbon nanomesh functionalized with ZnO nanowires to various concentration of SO_2 gas ranging from 50 ppb to 33ppm at 275°C (a) resistance change under various concentration of SO_2 (b) corresponding response versus SO_2 concentration.

The gas response comparison of the suspended carbon nanomesh functionalized with the ZnO nanowires gas sensor is shown in Figure 43, For the proper comparison of the response of each gas, all gases except CH_4 gas were compared based on the concentration of 2 ppm. As is well known, the response to NO_2 gas is much greater than the response to other gases. The response of $C_6H_6/CH_4/CO/H_2/SO_2$ gases was about 1 ~ 1.5 for 2 ppm concentration, while the response for 2 ppm NO_2 gas was 275, indicating that it has a very high selectivity for NO2 gas.

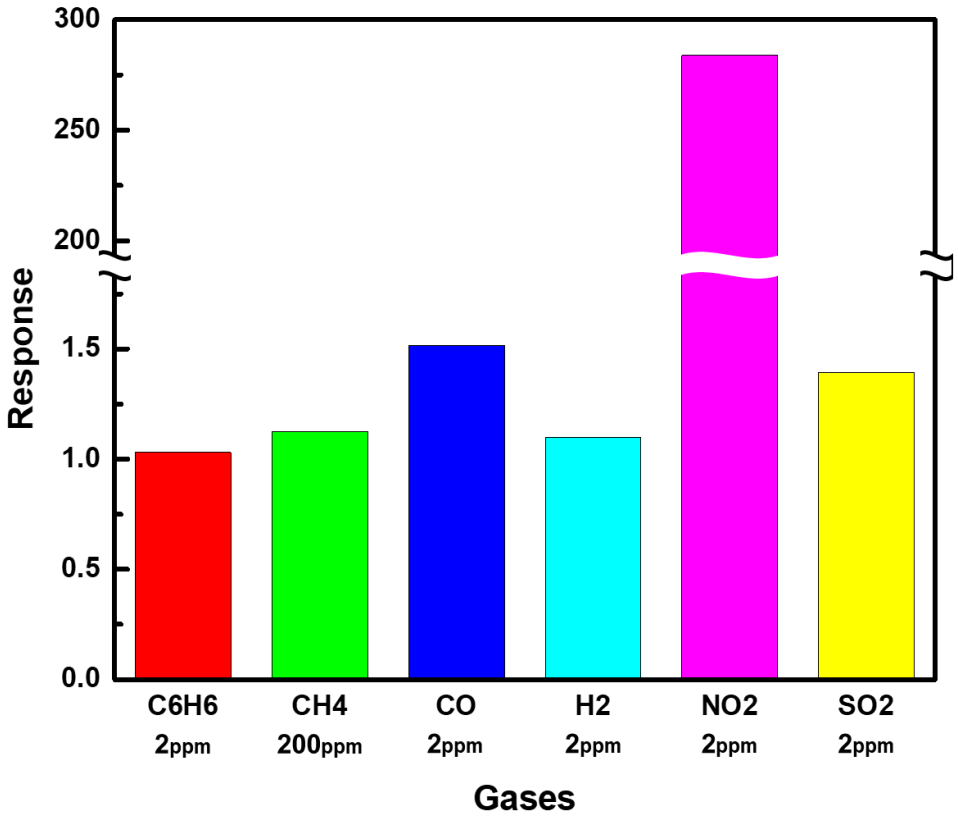

Figure 43. The comparison of gas responses of the suspended carbon nanomesh functionalized with ZnO nanowires to various gases of 2 ppm concentration (except for CH_4) at 275°C.

3.4.2 Sensor reliability

The reliability analysis of the sensor was made through the reproducibility and stability analysis of the sensor response. For the reproducibility analysis, NO_2 gas of 1/3/5 ppm was reacted in random order and the size of the response was reproducible with respect to the gas concentration. For a gas of 1/3/5ppm as shown in Figure 44, the response size was constantly around 5% error. This indicates that the sensor has the ability to show a promise response to continuously changing gas concentrations.

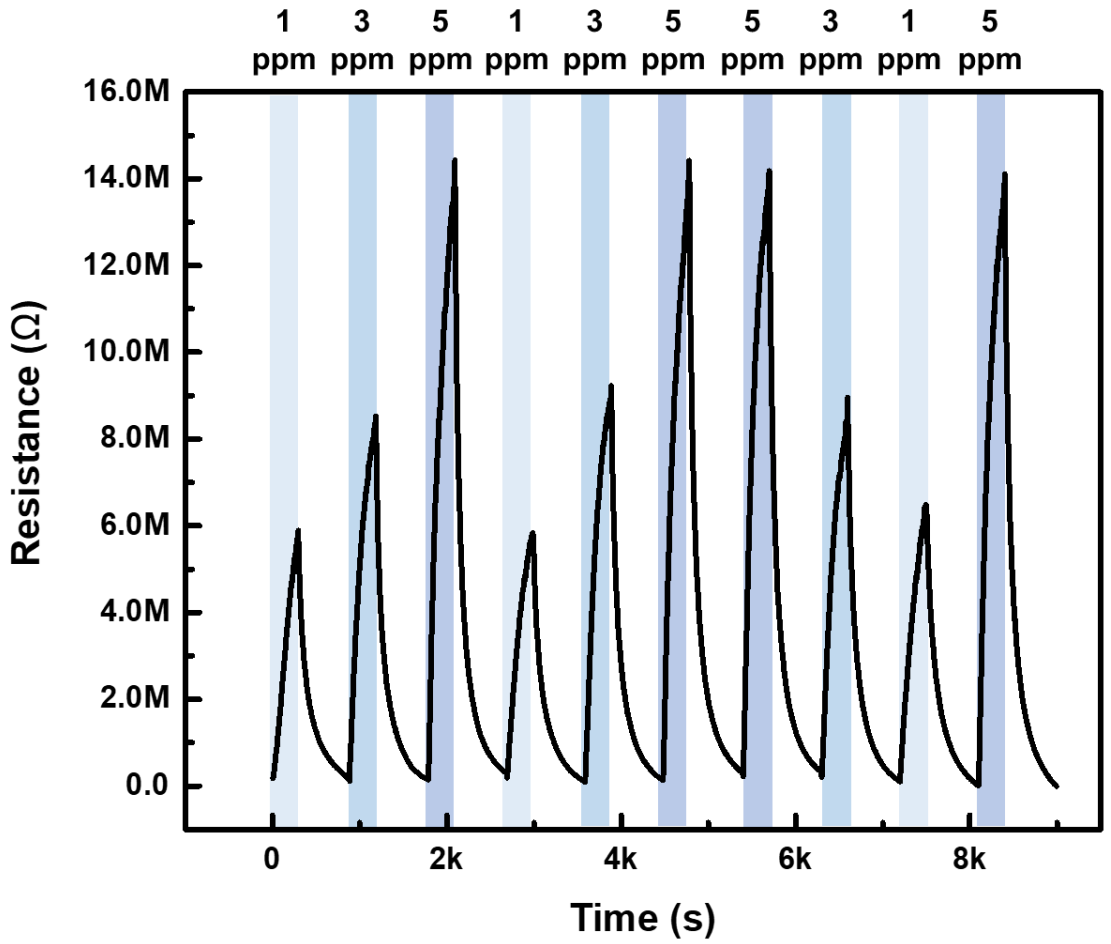

Figure 44. Reproducibility of the suspended carbon nanomesh functionalized with ZnO NWs under several cycles of different concentrations of NO_2 gas at 275ºC

In an analysis of the stability, the sensor was observed to change its response to the same concentration over a month. As shown in Figure 45, the NO_2 gas of 5 ppm showed almost the same reactivity in the one-month experiment. This indicates that the gas sensor proposed in this study can maintain reliable performance without significant decay effect over time.

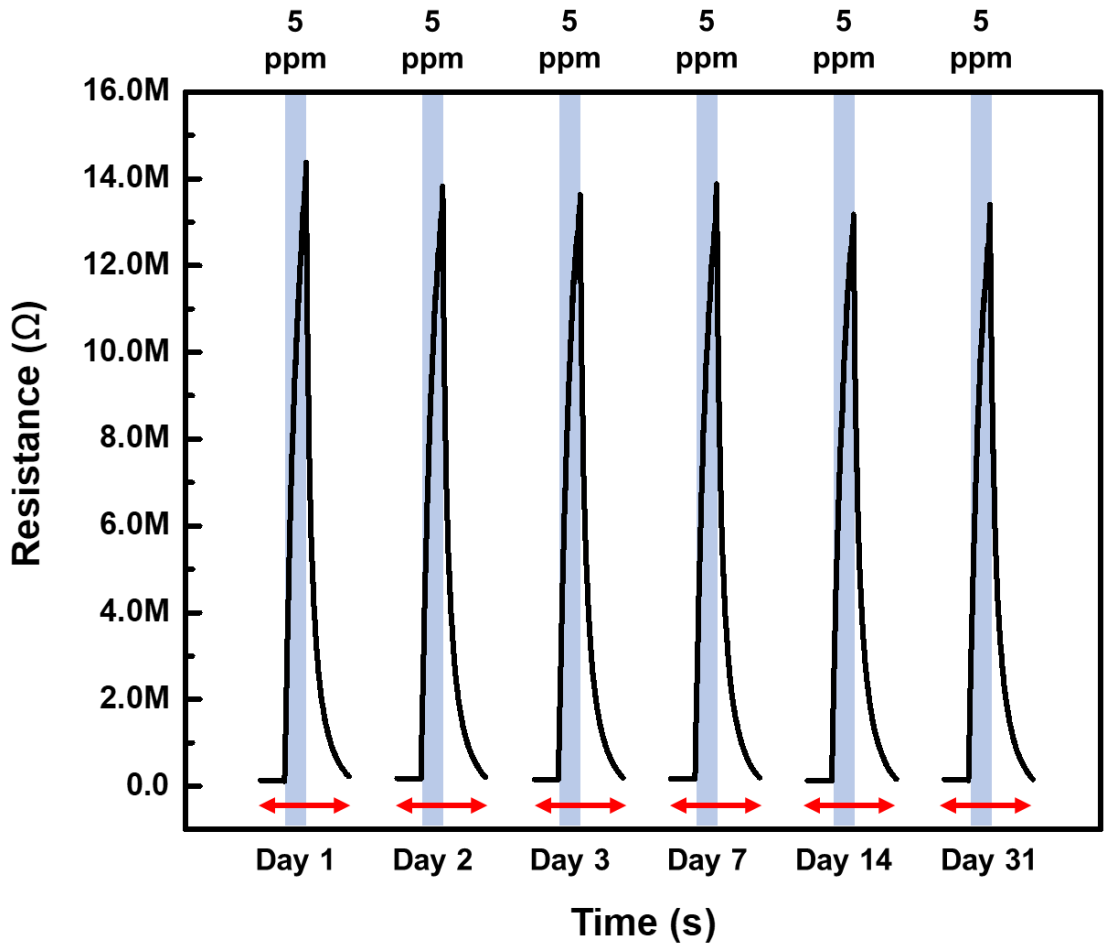

Figure 45. Long-term stability of the suspend carbon nanomesh functionalized with ZnO NWs: the gas response and recovery behaviors to 5ppm NO_2 gas at 275°C for a month.

4 Conclusion

In this research, a highly sensitive gas sensor based on suspended carbon nanomesh that facilitates 1-D metal oxide junctions is introduced. We demonstrated this sensor integrating ZnO NWs onto the suspended carbon nanomesh using batch fabrication viable processes including UV-lithography, C-MEMS, and hydrothermal metal oxide growth. The electrical resistivity of suspended carbon nanomesh is adjusted to a high value so that the measured resistance during the gas sensing experiment can be originated from almost ZnO portion even without any insulation layers to separate carbon circuit from ZnO portion circuit. By controlling the concentration of the hydrothermal growth solution, ZnO NW's diameter and length were tuned. Synthesized ZnO NWs were long enough to make junctions and thin enough to get high sensitivity. The high sensitivity and wide sensing range were achieved by making dense ZnO NW junctions over the suspended carbon nanomesh structure which act as an additional gas detection mechanism. Thanks to its suspended structure, the sensor response and recovery time were enhanced. Furthermore, high crystallinity of ZnO NWs ensured reliable sensor performance respect to reproducibility and long-term stability. Above all, this gas sensor based on suspended carbon nanomesh that facilitates 1-D metal oxide junctions is research the about basic platform of the gas sensor. Therefore, it is possible to design even better gas sensor models by applying any of the previously studied methodologies such as applying various metal oxide to build a sensor array or doping a noble metal. In conclusion, the gas sensor platform proposed in this study is a powerful and cost-effective gas sensor platform that can be extended in various directions.

Reference

[1] P. Mirtaheri, T. Omtveit, T. Klotzbuecher, S. Grimnes, O. G. Martinsen, T. I. Tonnessen, "Miniaturization of a biomedical gas sensor", *Physiol Meas*., **25**, 1511 - 1522 (2004).

[2] Keat, G.O, Kefeng, Z, C. A. Grimes, "A wireless, passive carbon nanotube-based gas sensor," *IEEE Sensors Journal*, **2**, 82 - 88 (2002)

[3] Fine, G.F., Cavanagh, L.M., Afonja, A., Binions, "R. Metal oxide semi-conductor gas sensors in environmental monitoring", *Sensors*, **10**, 5469 - 5502 (2010).

[4] T. Hübert, L. Boon-Brett, G. Black, and U. Banach, "Hydrogen sensors – A review", *Sensors and Actuators B: Chemical*, **157(2)**, 329 - 352 (2011)

[5] N. Funazaki, A. Hemmi, S. Ito, Y. Asano, Y. Yano, N. Miura, N. Yamazoe, "Application of semiconductor gas sensor to quality control of meat freshness in food industry", *Sensors and Actuators B: Chemical*, **25**, 797 - 800 (1995)

[6] S.V Ryabtsev, A.V Shaposhnick, A.N Lukin, E.P Domashevskaya, "Application of semiconductor gas sensors for medical diagnostics", *Sensors and Actuators B: Chemical*, **59**, 26 – 29 (1999)

[7] Peterson, P., Aujla, A., Grant, K. H., Brundle, A. G., Thompson, M. R., Vande Hey, J., Leigh, R. J., "Practical Use of Metal Oxide Semiconductor Gas Sensors for Measuring Nitrogen Dioxide and Ozone in Urban Environments", *Sensors*, **17**, 1653 (2017)

[8] Wales, D. J., Grand, J., Ting, V. P., Burke, R. D., Edler, K. J., Bowen, C. R., Mintova, S., Burrows, A. D., "Gas sensing using porous materials for automotive applications", *Chemical Society Reviews*, **44**, 4290 – 4321 (2015)

[9] Yamazoe, N. "New approaches for improving semiconductor gas sensors" *Sensors and Actuators B: Chemical*, **5**, 7 - 19 (1991)

[10] Y. Zainab, H. M. Nizar, K., Ahsanul, Awang, Z., "Gas Sensors: A Review", *Sensors and Transducers*. **168**, 61-75 (2014).

[11] H. Nazemi, A. Joseph, J. Park, A. Emadi, "Advanced Micro- and Nano-Gas Sensor Technology: A Review", *sensors*, **19**, 1285 (2019)

[12] S. Sharma, M. Madou, "A new approach to gas sensing with nanotechnology", *Philosophical transactions*, **370**, 2448 – 2473 (2012)

[13] J. C. Giselle, R. Jordi, F. X. Rius, "Gas sensors based on nanostructured materials". *The Analyst*., **132**, 1083 - 99 (2007)

[14] Li, N., Qiu, X., Wei, Y., Zhang, E., Wang, J., Li, C., Peng, Y., Wei, J., Meng, H., Wang, G., Zang, Z., "A portable low-power integrated current and temperature laser controller for high-sensitivity gas sensor applications", *Review of Scientific Instruments*, **89**, 103103–103114 (2018)

[15] V. Guidi, G. C. Cardinali, L. Dori, G. Faglia, M. Ferroni, G. Martinelli, P. Nelli, G. Sberveglieri, "Thin-film gas sensor implemented on a low-power-consumption micromachined silicon structure", *Sensors and Actuators B: Chemical*, **49**, 88 – 92 (1998)

[16] Kumar, R., Al-Dossary, O., Kumar, G., "Zinc Oxide Nanostructures for NO2 Gas–Sensor Applications: A Review", *Nano-Micro Letters*, **7**, 97 - 120 (2015)

[17] Huang J., Wan Q., "Gas Sensors Based on Semiconducting Metal Oxide One-Dimensional Nanostructures". *Sensors*, **9**, 9903 – 9924 (2009)

[18] J. Lee, "Gas sensors using hierarchical and hollow oxide nanostructures: Overview", *Sensors and Actuators B: Chemical*, **140**, 319 – 336 (2009)

[19] Q. Wan, Q. H. Li, Y. J. Chen, T. H. Wang, "Fabrication and ethanol sensing characteristics of ZnO nanowire gas sensors", *Applied Physics Letters*, **84**, 3654 (2004)

[20] X. Chen, Cell K.Y. Wong, C. A. Yuan, G. Zhang, "Nanowire-based gas sensors", *Sensors and Actuators B: Chemical*, **177**, 178 – 195 (2013)

[21] M. Tonezzer, N.V. Hieu, "Size-dependent response of single-nanowire gas sensors", *Sensors and Actuators B: Chemical*, **163**, 146 – 152 (2012)

[22] L. Valentini, I. Armentano, J. M. Kenny, "Sensors for sub-ppm NO_2 gas detection based on carbon nanotube thin films", *Applied Physics Letters*, **82**, 961 (2003)

[23] G. Sakai, N. Matsunaga, K. Shimanoe, N. Yamazoe, "Theory of gas-diffusion controlled sensitivity for thin film semiconductor gas sensor", *Sensors and Actuators B: Chemical*, **80**, 125 – 131 (2001)

[24] G Sberveglieri, "Recent developments in semiconducting thin-film gas sensors", *Sensors and Actuators B: Chemical*, **23**, 103 – 109 (1995)

[25] Z Li, Q Zhao, W Fan, J Zhan, "Porous SnO_2 nanospheres as sensitive gas sensors for volatile organic compounds detection", *Nanoscale*, **3**, 1646 – 1652 (2011)

[26] X Gou, G Wang, J Park, H Liu, J Yang, "Monodisperse hematite porous nanospheres: synthesis, characterization, and applications for gas sensors", *Nanotechnology*, **19**, 125606 (2008)

[27] N. Yamazoe, "Toward innovations of gas sensor technology", *Sensors and Actuators B: Chemical*, **108**, 2 – 14 (2005)

[28] W. Shin, M. Matsumiya, F. Qiu, N. Izu, N. Murayama, "Thermoelectric gas sensor for detection of high hydrogen concentration", *Sensors and Actuators B: Chemical*, **97**, 344 – 347 (2004)

[29] E.-B. Lee, I.-S. Hwang, J.-H. Cha, H.-J. Lee, W.-B. Lee, J. J. Pak, J.-H. Lee, and B.-K. Ju, "Micromachined catalytic combustible hydrogen gas sensor", *Sensors and Actuators B: Chemical*, **153**, 392 – 397 (2011)

[30] I. Simon, M. Arndt, "Thermal and gas-sensing properties of a micromachined thermal conductivity sensor for the detection of hydrogen in automotive applications", *Sensors and Actuators A: Physical*, **97**, 104 – 108 (2002)

[31] N. Dossi, R. Toniolo, A. Pizzariello, E. Carrilho, E. Piccin, S. Battiston, G. Bontempelli, "An electrochemical gas sensor based on paper supported room temperature ionic liquids", *Lab on a chip*, **12**, 153 – 158 (2012)

[32] MJ Tierney, H. Kim, "Electrochemical Gas Sensor with Extremely Fast Response Times", *Analytical Chemistry*, **65**, 3435 – 3440 (1993)

[33] H Li, X Mu, Y Yang, AJ Mason, "Low Power Multimode Electrochemical Gas Sensor Array System for Wearable Health and Safety Monitoring", *Sensors*, **14**, 3391 – 3399 (2014)

[34] Z Jin, Y Su, Y Duan, "Development of a polyaniline-based optical ammonia sensor", *Sensors and Actuators B: Chemical*, **72**, 75 – 79 (2001)

[35] F Tavoli, N Alizadeh, "Optical ammonia gas sensor based on nanostructure dye-doped polypyrrole", *Sensors and Actuators B: Chemical*, **176**, 761 – 767 (2013)

[36] SR Morrison, "Mechanism of semiconductor gas sensor operation", *Sensors and Actuators*, **11**, 283 – 287 (1987)

[37] Y. Kim, S. Ha, K. Kim, H. Yang, S. Choi, Y. Kim, "Room-temperature semiconductor gas sensor based on nonstoichiometric tungsten oxide nanorod film", *Applied Physics Letters*, **86**, 213105 (2005)

[38] N Yamazoe, G Sakai, K Shimanoe, "Oxide semiconductor gas sensors", *Catalysis Surveys from Asia*, **7**, 63 – 75 (2003)

[39] Y. Lee, H. Huang, O.K. Tan, M.S. Tse, "Semiconductor gas sensor based on Pd-doped SnO_2 nanorod thin films", *Sensors and Actuators B: Chemical*, **132**, 239 – 242 (2008)

[40] A. Dey, "Semiconductor metal oxide gas sensors", *Materials Science & Engineering B*, **229**, 206 – 217 (2018)

[41] N Hongsith, C Viriyaworasakul, P Mangkorntong, N.Mangkorntong, S.Choopun, "Ethanol sensor based on ZnO and Au-doped ZnO nanowires" *ceramic International*, **34**, 823 – 826 (2008)

[42] J. Moon, J. Park, S. Lee, T. Zyung, I. Kim, "Pd-doped TiO_2 nanofiber networks for gas sensor applications", *Sensors and Actuators B: Chemical*, **149**, 301 – 305 (2010)

[43] H Zhang, G Cao, Z Wang, Y Yang, Z Shi, Z Gu, "Growth of manganese oxide nanoflowers on vertically-aligned carbon nanotube arrays for high-rate electrochemical capacitive energy storage", *Nanoletters*, **8**, 2664 – 2668 (2008)

[44] GF Fine, LM Cavanagh, A Afonja, R Binions, "Metal oxide semi-conductor gas sensors in environmental monitoring", *Sensors*, **10**, 5469 – 5502 (2010)

[45] S.G. Chatterjee, S. Chatterjee, A.K. Ray, A.K. Chakraborty, "Graphene–metal oxide nanohybrids for toxic gas sensor: a review", *Sensors and Actuators B: Chemical*, **221**, 1170 – 1181 (2015)

[46] M. Ahn, K. Park, J. Heo, J. Park, D. Kim, K. Choi, J. Lee, S. Hong, "Gas sensing properties of defect-controlled ZnO-nanowire gas sensor", *Applied Physics Letters*, **93**, 263103 (2008)

[47] B. Wang, L.F. Zhu, Y.H. Yang, N.S. Xu, G.W. Yang, "Fabrication of a SnO2 Nanowire Gas Sensor and Sensor Performance for Hydrogen", *Journal of Physical Chemistry*, **112**, 6643 - 6647 (2008)

[48] M Ferroni, V Guidi, G Martinelli, G Faglia, P Nelli, G. Sberveglieri, "Characterization of a nanosized TiO_2 gas sensor", *Nanostructured Materials*, **7**, 709 - 718 (1996)

[49] G Korotcenkov, V Brinzari, A Cerneavschi, M Ivanov, V. Golovanov, A. Cornet, J. Morante, A. Cabot, J. Arbiol, "The influence of film structure on In_2O_3 gas response", *Thin Solid Films*, **460**, 315 - 323 (2004)

[50] Y. Kim, I. Hwang, S. Kim, C. Lee, J. Lee, "CuO nanowire gas sensors for air quality control in automotive cabin", *Sensors and Actuators B: Chemical*, **135**, 298 – 303 (2008)

[51] C Wang, L Yin, L Zhang, D Xiang, R Gao, "Metal oxide gas sensors: sensitivity and influencing factors", *Sensors*, **10**, 2088 – 2106 (2010)

[52] H. Kim, J. Lee, "Highly sensitive and selective gas sensors using p-type oxide semiconductors: Overview", *Sensors and Actuators B: Chemical*, **192**, 607 – 627 (2014)

[53] A Vaseashta, D Dimova-Malinovska, "Nanostructured and nanoscale devices, sensors and detectors", *Science and Technology of Advanced Materials*, **6**, 312 - 318 (2006)

[54] B. Huang, Z. Li, Z. Liu, G. Zhou, S. Hao, J. Wu, B. Gu, W. Duan, "Adsorption of Gas Molecules on Graphene Nanoribbons and Its Implication for Nanoscale Molecule Sensor", *Journal of Physical Chemistry*, **112**, 13442 - 13446 (2008)

[55] CJ Brinker, DR Dunphy, "Morphological control of surfactant-templated metal oxide films", *Current Opinion in Colloid & Interface Science*, **11**, 126 - 132 (2006)

[56] Y. Jun, J. Choi, J. Cheon, "Shape control of semiconductor and metal oxide nanocrystals through nonhydrolytic colloidal routes", *Angewandte Chemie International Edition*, **45**, 126 - 132 (2006)

[57] G. Korotcenkov, "Gas response control through structural and chemical modification of metal oxide films: state of the art and approaches", *Sensors and Actuators B: Chemical*, **107**, 209 – 232 (2005)

[58] R. Bogue, "MEMS sensors: past, present and future" *Sensor Review*, **27**, 7 – 13 (2007)

[59] K.D. Mitzner, J. Sternhagen, D.W. Galipea, "Development of a micromachined hazardous gas sensor array", *Sensors and Actuators B: Chemical*, **93**, 92 – 99 (2003)

[60] H. Meixner, J. Gerblinger, U. Lampe, M. Fleischer, "Thin-film gas sensors based on semiconducting metal oxides", *Sensors and Actuators B: Chemical*, **23**, 119 – 125 (1995)

[61] J.A. Dirksen, K. Duval, T.A. Ring, "NiO thin-film formaldehyde gas sensor", *Sensors and Actuators B: Chemical*, **80**, 106 – 115 (2001)

[62] V. Balouria, N.S. Ramgir, A. Singh, A.K. Debnath, A. Mahajan, R.K. Bedia, D.K. Aswalb, S.K. Guptab, "Enhanced H_2S sensing characteristics of Au modified Fe_2O_3 thin films", *Sensors and Actuators B: Chemical*, **219**, 125 – 132 (2015)

[63] N.S. Ramgir, Y. Hwang, S. Jhung, H. Kim, J. Hwang, I.S. Mulla, "CO sensor derived from mesostructured Au-doped SnO2 thin film", *Applied Surface Science*, **252**, 4298 – 4305 (2006)

[64] H. Yu, T. Yang, R. Zhao, B. Xiao, Z. Li, M. Zhang, "Fast formaldehyde gas sensing response properties of ultrathin SnO 2 nanosheets", *RSC Advances*, **5**, 104574 – 104581 (2015)

[65] C. Young, .J Wang, J. Kim, Y. Sugahara, J. Henzie, "Controlled Chemical Vapor Deposition for Synthesis of Nanowire Arrays of Metal–Organic Frameworks and Their Thermal Conversion to Carbon/Metal Oxide Hybrid Materials", *Chemical Materials*, **30**, 3379 - 3386 (2018)

[66] J.E. Graves, M.E.A. Bowker, A. Summer, A. Greenwood, C. Ponce de León, F.C. Walsh, "A new procedure for the template synthesis of metal nanowires", *Electrochemistry Communications*, **87**, 58 – 62 (2018)

[67] O. Lupan, V. Postica, V. Cretu, N. Wolff, V. Duppel, L. Kienle, R. Adelung, "Single and networked CuO nanowires for highly sensitive p-type semiconductor gas sensor applications", *physica status solidi (RRL)*, **10**, (2015)

[68] B. Liu, H.C. Zeng, "Hydrothermal synthesis of ZnO nanorods in the diameter regime of 50 nm", *Journal of the American Chemical Society*, **125**, 4430 – 4431 (2003)

[69] S. Santra, P.K. Guha, S.Z. Ali, P. Hiralal, H.E. Unalan, J.A. Covington, G.A.J. Amaratunga, W.I. Milne, J.W. Gardner, F. Udrea, "ZnO nanowires grown on SOI CMOS substrate for ethanol sensing", *Sensors and Actuators B: Chemical*, **146**, 559 – 565 (2010)

[70] X. Lai, J. Li, B.A. Korgel, Z. Dong, Z. Li, F. Su, J. Du, D. Wang, "General Synthesis and Gas-Sensing Properties of Multiple-Shell Metal Oxide Hollow Microspheres", *Angewandte Chemie International Edition*, **50**, (2011)

[71] J. Park, X. Shen, G. Wang, "Solvothermal synthesis and gas-sensing performance of Co3O4 hollow nanospheres", *Sensors and Actuators B: Chemical*, **136**, 494 – 498 (2009)

[72] J. Zhang, J. Liu, Q. Peng, X. Wang, Y. Li, "Nearly Monodisperse Cu2O and CuO Nanospheres: Preparation and Applications for Sensitive Gas Sensors", *Chemistry of materials*, **18**, 867 – 871 (2006)

[73] P. Samarasekara, N. Kumara, N.U.S. Yapa "Sputtered copper oxide (CuO) thin films for gas sensor devices", *Journal of Physics: Condensed Matter*, (2006)

[74] Y. Mo, Y. Okawa, M. Tajima, T. Nakai, N. Yoshiike, K. Natukawa, "Micro-machined gas sensor array based on metal film micro-heater", *Sensors and Actuators B: Chemical*, **79**, 175 – 181 (2001)

[75] Y. Lim, J. Heo, M. Madou, H. Shin, "Monolithic carbon structures including suspended single nanowires and nanomeshes as a sensor platform", *Nanoscale Research Letters*, **8**, 492 (2013)

[76] D. Baek, J. Choi, J. Kim, "Fabrication of suspended nanowires for highly sensitive gas sensing", *Sensors and Actuators B: Chemical*, **284**, 362 – 368 (2019)

[77] M. Ahn, K. Park, J. Heo, D. Kim, K. Choi, J. Park, "On-chip fabrication of ZnO-nanowire gas sensor with high gas sensitivity", *Sensors and Actuators B: Chemical*, **138**, 168 – 173 (2009)

[78] R. Khan, H.W. Ra, J. Kim, W. Jang, D. Sharma, Y. Im "Nanojunction effects in multiple ZnO nanowire gas sensor", *Sensors and Actuators B: Chemical*, **150**, 389 – 393 (2010)

[79] Y. Lim, S. Kim, Y. Kwon, J. Baik, H. Shin, "A highly sensitive gas-sensing platform based on a metal-oxide nanowire forest grown on a suspended carbon nanowire fabricated at a wafer level", *Sensors and Actuators B: Chemical*, **260**, 55 – 62 (2018)

[80] Y. Lim, Y. Lee, J. Heo, H. Shin, "Highly sensitive hydrogen gas sensor based on a suspended palladium/carbon nanowire fabricated via batch microfabrication processes", *Sensors and Actuators B: Chemical*, **210**, 218 – 224 (2015)

[81] C. Wang, G Jia, L.H. Taherabadi, M. Madou, "A novel method for the fabrication of high-aspect ratio C-MEMS structures", *Journal of Microelectromechanical Systems*, **14**, 348 – 358 (2005)

[82] C. Wang, M. Madou, "From MEMS to NEMS with carbon", *Biosensors and Bioelectronics*, **20**, 2181 – 2187 (2005)

[83] E.S. Kumar, M. Chandran, F. Bellarmine, R. Mannam, D. Nakamura, M. Higashihata, T. Okada, M. S. R. Rao, "Formation of one-dimensional ZnO nanowires from screw-dislocation-driven two-dimensional hexagonal stacking on diamond substrate using nanoparticle-assisted pulsed laser deposition", Journal of Physics D: Applied Physics, 23, (2013)

[84] S. Yi, S. Choi, J. Jang, J. Kim, W. Jung, "Low-temperature growth of ZnO nanorods by chemical bath deposition", Journal of Colloid and Interface Science, 313, 705 – 710 (2007)

[85] S. Pati, A. Maity, P. Banerji, S.B. Majumder, "Temperature dependent donor–acceptor transition of ZnO thin film gas sensor during butane detection", Sensors and Actuators B: Chemical, 183, 172 – 178 (2013)

[86] N.J. Nicholas, G.V. Franks, W.A. Ducker, "The mechanism for hydrothermal growth of zinc oxide", CrystEngComm, 14, 1232 – 1240 (2012)

[87] K. Edalati, A. Shakiba, J. Vahdati-Khaki, S.M. Zebarjada , "Low-temperature hydrothermal synthesis of ZnO nanorods: Effects of zinc salt concentration, various solvents and alkaline mineralizers", Materials Research Bulletin, 74, 374 – 379 (2016)

[88] K. H. Tam, C. K. Cheung, Y. H. Leung, A. B. Djurišić, C. C. Ling, C. D. Beling, S. Fung, W. M. Kwok, W. K. Chan, D. L. Phillips, L. Ding, W. K. Ge, "Defects in ZnO nanorods prepared by a hydrothermal method", The Journal of Physical Chemistry B, 110, 20865 – 20871 (2006)

[89] H. Clevenson, P. Desjardins, X. Gan, D. Englund, "High sensitivity gas sensor based on high-Q suspended polymer photonic crystal nanocavity", Applied Physics Letters , 104, 241108 (2014)

[90] H. Jung, Y. Kim, K. Jung, H. Im, Y.A. Pashkin, O. Astafiev, Y. Nakamura, H. Lee, Y. Miyamoto, J. S. Tsai, "Potential barrier modification and interface states formation in metal-oxide-metal tunnel junctions", Physical Review B, 80, 125413 (2009)

Acknowledgements

I would like to express my sincere gratitude to my advisor, Professor Heungjoo Shin. He always guided me continuously and convincingly all the time so that I could become a better researcher. Without his supports, I couldn't finish this thesis. The opportunity to have a degree under his guidance was a great fortune to me. I also appreciate to the committee members, Professor Jaesung Jang and Professor Hooneui Jeong for their insightful advice for my research. Thanks to them, I could successfully complete my thesis.

And I want to give thanks to our MNIS lab members, PoliceAnil Kumar Reddy, KunduPijus, Jongmin Lee, Beomsang Kim, Sanghee Jung, Taejung Kim, and Wootaek Cho. I really appreciate their continuous help and consideration. Also, I appreciate to graduated seniors, Youngjin Lim, Junyoung Seo and Soosung Kim. Even after they graduated and left, they gave me a lot of advice and encouragement. It was great luck to meet them as my senior researchers.

Also, I want to give thanks to my old friends, Eunhyeok Lim and Taegu Lee. I really appreciate them for always listening to me and cheering me up. And I am thankful to my Incheon friends Jinhyeok Yu, Sanghyuk Yun, Janggeun Lee, Haechan Jang, Changmin Choi, Handong Choi and Hyeonseok Choi for cheering me up even though it was hard to meet them. I also express my thanks to my TONGSU friends Heewon Kwak, Gunho Lee, Dongje Lee, Yunho Cho, and Samhoe Heo for playing, chatting and drinking with me. It was a great refreshment of my life at UNIST.

Above all, I would like to thank my family for supporting me with infinite love. They are the biggest reason I live. Thanks to them, I could finish my master's course.

I return my grateful acknowledgment to all these precious people of mine.